DESY-17-077
July 20, 2017

Studies of the diffractive photoproduction of isolated photons at HERA

ZEUS Collaboration

Abstract

The photoproduction of isolated photons has been measured in diffractive events recorded by the ZEUS detector at HERA. Cross sections are evaluated in the photon transverse-energy and pseudorapidity ranges $5 < E_T^\gamma < 15$ GeV and $-0.7 < \eta^\gamma < 0.9$, inclusively and also with a jet with transverse energy and pseudorapidity in the ranges $4 < E_T^{\rm jet} < 35$ GeV and $-1.5 < \eta^{\rm jet} < 1.8$, using a total integrated electron–proton luminosity of 456 pb^{-1}. A number of kinematic variables were studied and compared to predictions from the Rapgap Monte Carlo model. An excess of data is observed above the Rapgap predictions for $z_{I\!P}^{\rm meas} > 0.9$, where $z_{I\!P}^{\rm meas}$ is the fraction of the longitudinal momentum of the colourless "Pomeron" exchange that is transferred to the photon–jet final state, giving evidence for direct Pomeron interactions.

The ZEUS Collaboration

H. Abramowicz[24,o], I. Abt[19], L. Adamczyk[7], M. Adamus[30], S. Antonelli[1], V. Aushev[16], Y. Aushev[16], O. Behnke[9], U. Behrens[9], A. Bertolin[21], I. Bloch[10], I. Brock[2], N.H. Brook[28,p], R. Brugnera[22], A. Bruni[1], P.J. Bussey[11], A. Caldwell[19], M. Capua[4], C.D. Catterall[32], J. Chwastowski[6], J. Ciborowski[29,r], R. Ciesielski[9,d], A.M. Cooper-Sarkar[20], M. Corradi[1,a], R.K. Dementiev[18], R.C.E. Devenish[20], S. Dusini[21], B. Foster[12,i], G. Gach[7], E. Gallo[12,j], A. Garfagnini[22], A. Geiser[9], A. Gizhko[9], L.K. Gladilin[18], Yu.A. Golubkov[18], G. Grzelak[29], M. Guzik[7], C. Gwenlan[20], O. Hlushchenko[16,m], D. Hochman[31], R. Hori[13], Z.A. Ibrahim[5], Y. Iga[23], M. Ishitsuka[25], N.Z. Jomhari[5], I. Kadenko[16], S. Kananov[24], U. Karshon[31], P. Kaur[3,b], D. Kisielewska[7], R. Klanner[12], U. Klein[9,e], I.A. Korzhavina[18], A. Kotański[8], N. Kovalchuk[12], H. Kowalski[9], B. Krupa[6], O. Kuprash[9,f], M. Kuze[25], B.B. Levchenko[18], A. Levy[24], M. Lisovyi[9,g], E. Lobodzinska[9], B. Löhr[9], E. Lohrmann[12], A. Longhin[21], O.Yu. Lukina[18], J. Malka[9], A. Mastroberardino[4], F. Mohamad Idris[5,c], N. Mohammad Nasir[5], V. Myronenko[9,h], K. Nagano[13], Yu. Onishchuk[16], E. Paul[2], W. Perlański[29,s], N.S. Pokrovskiy[14], A. Polini[1], M. Przybycień[7], M. Ruspa[27], D.H. Saxon[11], M. Schioppa[4], U. Schneekloth[9], T. Schörner-Sadenius[9], L.M. Shcheglova[18,n], O. Shkola[16], Yu. Shyrma[15], I.O. Skillicorn[11], W. Słomiński[8], A. Solano[26], L. Stanco[21], N. Stefaniuk[9], A. Stern[24], P. Stopa[6], J. Sztuk-Dambietz[12,k], E. Tassi[4], K. Tokushuku[13], J. Tomaszewska[29,t], T. Tsurugai[17], M. Turcato[12,k], O. Turkot[9,h], T. Tymieniecka[30], A. Verbytskyi[19], W.A.T. Wan Abdullah[5], K. Wichmann[9,h], M. Wing[28,q], S. Yamada[13], Y. Yamazaki[13,l], A.F. Żarnecki[29], L. Zawiejski[6], O. Zenaiev[9], B.O. Zhautykov[14]

[1] *INFN Bologna, Bologna, Italy* [A]

[2] *Physikalisches Institut der Universität Bonn, Bonn, Germany* [B]

[3] *Panjab University, Department of Physics, Chandigarh, India*

[4] *Calabria University, Physics Department and INFN, Cosenza, Italy* [A]

[5] *National Centre for Particle Physics, Universiti Malaya, 50603 Kuala Lumpur, Malaysia* [C]

[6] *The Henryk Niewodniczanski Institute of Nuclear Physics, Polish Academy of Sciences, Krakow, Poland*

[7] *AGH University of Science and Technology, Faculty of Physics and Applied Computer Science, Krakow, Poland*

[8] *Department of Physics, Jagellonian University, Krakow, Poland*

[9] *Deutsches Elektronen-Synchrotron DESY, Hamburg, Germany*

[10] *Deutsches Elektronen-Synchrotron DESY, Zeuthen, Germany*

[11] *School of Physics and Astronomy, University of Glasgow, Glasgow, United Kingdom* [D]

[12] *Hamburg University, Institute of Experimental Physics, Hamburg, Germany* [E]

[13] *Institute of Particle and Nuclear Studies, KEK, Tsukuba, Japan* [F]

[14] *Institute of Physics and Technology of Ministry of Education and Science of Kazakhstan, Almaty, Kazakhstan*

[15] *Institute for Nuclear Research, National Academy of Sciences, Kyiv, Ukraine*

[16] *Department of Nuclear Physics, National Taras Shevchenko University of Kyiv, Kyiv, Ukraine*

[17] *Meiji Gakuin University, Faculty of General Education, Yokohama, Japan* [F]

[18] *Lomonosov Moscow State University, Skobeltsyn Institute of Nuclear Physics, Moscow, Russia* [G]

[19] *Max-Planck-Institut für Physik, München, Germany*

[20] *Department of Physics, University of Oxford, Oxford, United Kingdom* [D]

[21] *INFN Padova, Padova, Italy* [A]

[22] *Dipartimento di Fisica e Astronomia dell' Università and INFN, Padova, Italy* [A]

[23] *Polytechnic University, Tokyo, Japan* [F]

[24] *Raymond and Beverly Sackler Faculty of Exact Sciences, School of Physics, Tel Aviv University, Tel Aviv, Israel* [H]

[25] *Department of Physics, Tokyo Institute of Technology, Tokyo, Japan* [F]

[26] *Università di Torino and INFN, Torino, Italy* [A]

[27] *Università del Piemonte Orientale, Novara, and INFN, Torino, Italy* [A]

[28] *Physics and Astronomy Department, University College London, London, United Kingdom* [D]

[29] *Faculty of Physics, University of Warsaw, Warsaw, Poland*

[30] *National Centre for Nuclear Research, Warsaw, Poland*

[31] *Department of Particle Physics and Astrophysics, Weizmann Institute, Rehovot, Israel*

[32] *Department of Physics, York University, Ontario, Canada M3J 1P3* [I]

[A] supported by the Italian National Institute for Nuclear Physics (INFN)

[B] supported by the German Federal Ministry for Education and Research (BMBF), under contract No. 05 H09PDF

[C] supported by HIR grant UM.C/625/1/HIR/149 and UMRG grants RU006-2013, RP012A-13AFR and RP012B-13AFR from Universiti Malaya, and ERGS grant ER004-2012A from the Ministry of Education, Malaysia

[D] supported by the Science and Technology Facilities Council, UK

[E] supported by the German Federal Ministry for Education and Research (BMBF), under contract No. 05h09GUF, and the SFB 676 of the Deutsche Forschungsgemeinschaft (DFG)

[F] supported by the Japanese Ministry of Education, Culture, Sports, Science and Technology (MEXT) and its grants for Scientific Research

[G] partially supported by RF Presidential grant NSh-7989.2016.2

[H] supported by the Israel Science Foundation

[I] supported by the Natural Sciences and Engineering Research Council of Canada (NSERC)

[a] now at INFN Roma, Italy

[b] now at Sant Longowal Institute of Engineering and Technology, Longowal, Punjab, India

[c] also at Agensi Nuklear Malaysia, 43000 Kajang, Bangi, Malaysia

[d] now at Rockefeller University, New York, NY 10065, USA

[e] now at University of Liverpool, United Kingdom

[f] now at Tel Aviv University, Israel

[g] now at Physikalisches Institut, Universität Heidelberg, Germany

[h] supported by the Alexander von Humboldt Foundation

[i] Alexander von Humboldt Professor; also at DESY and University of Oxford

[j] also at DESY

[k] now at European X-ray Free-Electron Laser facility GmbH, Hamburg, Germany

[l] now at Kobe University, Japan

[m] now at RWTH Aachen, Germany

[n] also at University of Bristol, United Kingdom

[o] also at Max Planck Institute for Physics, Munich, Germany, External Scientific Member

[p] now at University of Bath, United Kingdom

[q] also supported by DESY and the Alexander von Humboldt Foundation

[r] also at Łódź University, Poland

[s] member of Łódź University, Poland

[t] now at Polish Air Force Academy in Deblin

1 Introduction

Diffractive interactions are a distinctive class of hadronic interactions in which the scattering of the incoming particle is mediated by an exchanged object carrying no quantum numbers, commonly referred to as the Pomeron. Such processes are typically characterised by a forward nucleon or nucleonic state that is separated by a gap in rapidity from the hadronic final state produced in the central region of the event. At the HERA ep collider, diffractive processes have been studied both in photoproduction and in deep inelastic scattering (DIS), photoproduction processes being those in which the exchanged photon is quasi-real. The virtuality Q^2 of the exchanged photon is typically much smaller than 1 GeV^2 in photoproduction processes, which constitute a large majority of the ep collisions. Events with $Q^2 > 1\,\text{GeV}^2$ are conventionally regarded as DIS.

The physical nature of the Pomeron is not fully established within quantum chromodynamics (QCD), and a number of models have been proposed [1–3]. In an approach originated by Ingelman and Schlein [4], the Pomeron is taken to be a hadron-like object that contains quarks and gluons. The Pomeron parton density functions (PDFs) can be evaluated from fits to DIS data [5]. In an alternative approach [2], the Pomeron is equivalent to the exchange of two gluons.

The photon–Pomeron interaction can take place through processes in which the photon or Pomeron acts as a source of quarks and gluons, which then take part in the QCD scatter (resolved processes) and processes in which the photon or Pomeron interacts as a whole (direct processes). There are thus in principle four different types of process that may be experimentally studied: a direct or resolved photon interacting with a direct or resolved Pomeron. Examples of these processes are illustrated in Fig. 1. Direct Pomeron processes are not included in the Ingelman–Schlein model, but are taken into account in other approaches [6]. Within the Ingelman–Schlein framework, it is normally assumed that a Pomeron with a universal set of PDFs is emitted, making allowance for QCD evolution effects. In the H1 DIS analysis [5], the results of which are used here, the Pomeron PDFs are dominated by gluons in most regions of parameter space, but a significant quark content is also present. If the factorisation hypothesis holds, the same parton structure would be valid both in direct photoproduction processes and in DIS, although in resolved photon processes, absorptive effects may be present [7–9].

Several studies of diffractive dijet events in photoproduction and DIS have been carried out at HERA [10–15]. The present paper gives measurements of diffractive events in which a hard isolated "prompt" photon is detected in the central region of the ZEUS detector and may be accompanied by one or more jets. Such processes, while rare, are interesting for a number of reasons. The four different types of direct and resolved processes can be identified, in particular direct Pomeron interactions. The prompt photon must originate

from a charged parton, and its observation therefore demonstrates the presence either of a quark in the Pomeron or of higher-order processes in which both the Pomeron and the incident photon couple to quarks. This contrasts with diffractive dijet production, which is mainly sensitive to the gluon content of the Pomeron.

Hard photons are also produced in "fragmentation processes" in which a photon is radiated within a jet. Such processes can be suppressed by requiring the observed hard photon to be isolated from other particles in the event.

The H1 collaboration previously measured inclusive diffractive high-energy prompt photons as a function of their transverse momentum, but in a different kinematic region from the present work [16]. Analyses of isolated hard photons in non-diffractive photoproduction have been presented by the ZEUS and H1 collaborations [17–23], as well as in DIS [24–27].

2 The ZEUS detector

The analysis presented here is based on two data samples corresponding to integrated luminosities of 82 and 374 pb^{-1}, taken during the years 1998–2000 and 2004–2007, respectively, with the ZEUS detector at HERA. These are referred to as HERA-I and HERA-II samples. During these periods, HERA ran with electron and positron beams[1] of energy $E_e = 27.5$ GeV and a proton beam of energy $E_p = 920$ GeV.

A detailed description of the ZEUS detector[2] can be found elsewhere [28]. Charged particles were measured in the central tracking detector (CTD) [29] and, in HERA-II, in a silicon microvertex detector [30]. These operated in a magnetic field of 1.43 T provided by a thin superconducting solenoid. The high-resolution uranium–scintillator calorimeter (CAL) [31] consisted of three parts: the forward (FCAL), the barrel (BCAL) and the rear (RCAL) calorimeters. The BCAL covered the pseudorapidity range -0.74 to 1.10 as seen from the nominal interaction point, and the FCAL and RCAL extended the coverage to the range -3.5 to 4.0. Each part of the CAL was subdivided into elements referred to as cells. The barrel electromagnetic calorimeter (BEMC) cells had a pointing geometry directed at the nominal interaction point, and were approximately $5 \times 20\,\text{cm}^2$ in cross section, with the finer granularity in the Z direction and the coarser in the (X, Y) plane.

[1] Hereafter, "electron" refers to both electrons and positrons.

[2] The ZEUS coordinate system is a right-handed Cartesian system, with the Z axis pointing in the nominal proton beam direction, referred to as the "forward direction", and the X axis pointing towards the centre of HERA. The coordinate origin is at the centre of the central tracking detector. The pseudorapidity is defined as $\eta = -\ln\left(\tan\frac{\theta}{2}\right)$, where the polar angle, θ, is measured with respect to the Z axis.

This fine granularity allows the use of shower-shape distributions to distinguish isolated photons from the products of neutral meson decays such as $\pi^0 \to \gamma\gamma$. The CAL energy resolution, as measured under test-beam conditions, was $\sigma(E)/E = 0.18/\sqrt{E}$ for electrons and $0.35/\sqrt{E}$ for hadrons, where E is in GeV.

In most HERA events, the outgoing electron passes inside the inner aperture of the RCAL, corresponding to a scattering angle of approximately 70 mrad with an upper limit on Q^2 of the order of 1 GeV^2. The absence of a detected electron corresponds to a good approximation to a photoproduction event.

During the HERA-I running, the aperture between the proton beam pipe and the surrounding FCAL was occupied by the forward plug calorimeter (FPC), which extended the rapidity coverage to +5.0 [32]. In particular, it improved the reliability of the measurement of the rapidity gap in diffractive events. During the HERA-II running, the configuration of this region was altered and a beam-focusing magnet occupied the place of the FPC.

The luminosity was measured [33] using the reaction $ep \to e\gamma p$ by a luminosity detector which for HERA-I running consisted of a lead–scintillator calorimeter [34] and for HERA-II running consisted of two independent systems: the lead–scintillator calorimeter and a magnetic spectrometer [35].

3 Effects of proton dissociation

Diffractive events are characterised by a rapidity gap between the forward proton, or dissociated-proton system, and the rest of the particles in the event. A sample of diffractive events may be obtained by excluding the events in which particles are recorded in the forward regions of the detector beyond a maximum pseudorapidity value, $\eta_{\max}$, taken as 2.5 in the present analysis. The forward-scattered proton is not detected; however the accepted event sample includes contributions in which the proton emerges in a dissociated state whose products pass undetected inside the central aperture of the FCAL or FPC. In some cases, wider-angle dissociation products may be detected and cause the event to fail the diffractive selections.

The HERA-I and HERA-II detector configurations differ in their ability to identify events with proton dissociation. For the HERA-I data, the use of the FPC allowed most of these events to be rejected, but the recorded cross sections still include a contribution from undetected dissociated-proton systems with masses up to approximately 3 GeV. In the analysis of diffractive dijet events in photoproduction, this was evaluated to be $16 \pm 4\%$ of the total published diffractive cross section [12]. For the HERA-II data, the size of the central aperture of the FCAL was doubled. This, together with the absence of the FPC

and the possibility of secondary scattering from the beam-focusing magnet, generated two effects which act in opposite directions. In the first of these, the measured differential cross sections include a larger contribution from proton dissociation; in the analysis of diffractive dijet production in DIS, using $\eta_{\max} = 2.0$, this contribution was evaluated to be $45 \pm 15\%$ and comprises dissociated-proton systems with masses up to approximately 6 GeV [36]. A similar contribution would be expected in diffractive photoproduction. It affects only the normalisation of the differential cross sections, if the principle of vertex factorisation is assumed to hold. However, it was possible for particles within a dissociated-proton system to scatter from the focusing magnet into the detector. This effect was not accurately simulatable. It can reduce the fraction of proton-dissociated events in the sample by removing the forward rapidity gap in some of the events.

The higher statistics available in the HERA-II running made this data set suitable for studying the distributions of kinematic variables, which are described in Section 4. However the possible presence of a substantial number of events with proton dissociation should be allowed for in the measured cross sections. The HERA-I data set, being less affected by the proton dissociation and with the focusing magnet absent, was used to evaluate an integrated "visible" cross section taken over the observed ranges of the measured variables.

4 Measured variables

All the measured quantities used in this analysis were determined in the laboratory frame. In direct photon processes in photoproduction, the incoming virtual photon is absorbed by a quark from the target particle, here a Pomeron, while in resolved photon processes, the virtual photon's hadronic structure provides a quark or gluon that interacts with a quark or gluon from the Pomeron. These two classes of process, which are unambiguously defined only at the leading order (LO) of QCD, may be partially distinguished in events containing a high-E_T photon and a jet by means of the quantity

$$x_\gamma^{\text{meas}} = \frac{E^\gamma + E^{\text{jet}} - p_Z^\gamma - p_Z^{\text{jet}}}{E^{\text{all}} - p_Z^{\text{all}}}, \tag{1}$$

which measures the fraction of the incoming photon energy that is given to the outgoing photon and jet. The quantities E^γ and E^{jet} denote the energies of the outgoing photon and the jet, respectively, and p_Z denotes the corresponding longitudinal momenta. The suffix "all" refers to all objects that are measured in the detector or, in the case of simulations at the hadron level, all final-state particles except for the scattered beam electron and the outgoing proton. Events with a detected final-state electron are excluded from this analysis.

At LO, $x_\gamma^{\rm meas} = 1$ for direct photon events, while resolved photon events can have any value in the range (0, 1). Direct photon events at higher order can have $x_\gamma^{\rm meas}$ less than unity, but the presence of the LO processes generates a prominent peak in the observed cross section at high values of $x_\gamma^{\rm meas}$.

When the proton radiates a Pomeron that interacts with an incoming photon, the fraction of the proton energy carried by the radiated Pomeron is given to a good approximation by:

$$x_{I\!P} = (E^{\rm all} + p_Z^{\rm all})/2E_p, \tag{2}$$

where E_p is the energy of the proton beam.

The mass of the observed system, excluding the forward proton and its possible dissociation products but including all the reaction products of the incoming photon and Pomeron, is evaluated as:

$$M_X = \sqrt{(E^{\rm all})^2 - (p_Z^{\rm all})^2}. \tag{3}$$

The Pomeron may be described analogously to the photon [1, 6]. The fraction of the Pomeron energy that takes part in the hard interaction that generates the outgoing photon and jet is given by [10]:

$$z_{I\!P}^{\rm meas} = \frac{E^\gamma + E^{\rm jet} + p_Z^\gamma + p_Z^{\rm jet}}{E^{\rm all} + p_Z^{\rm all}}, \tag{4}$$

where the quantities are as before[3], and $z_{I\!P}^{\rm meas} = 1$ corresponds to direct Pomeron events, which are equivalent to the presence of a delta-function in the PDFs at $z_{I\!P}^{\rm meas} = 1$ [1, 6]. An event whose observed final state consists only of a prompt photon and a jet has $x_\gamma^{\rm meas} = z_{I\!P}^{\rm meas} = 1$.

Further variables that are used are as follows. A measurable approximation for the fraction y of the incoming electron energy that is transferred to the exchanged virtual photon is the Jacquet–Blondel variable, $y_{\rm JB}$ [37], where in the present analysis

$$y_{\rm JB} = \sum_i E_i(1 - \cos\theta_i)/2E_e. \tag{5}$$

Here, E_i is the energy of the i-th CAL cell, θ_i is its polar angle and the sum runs over all cells [38]. The photon–proton centre-of-mass energy, W, is calculated as

$$W = \sqrt{4yE_pE_e + m_p^2}, \tag{6}$$

where the small finite value of Q^2 is neglected, m_p is the proton mass and, at the detector level, y is replaced by $y_{\rm JB}$.

[3] The alternative formulation $z_{I\!P}^{\rm obs} = (E_T^\gamma \exp\eta^\gamma + E_T^{\rm jet} \exp\eta^{\rm jet})/(E^{\rm all} + p_Z^{\rm all})$, where E_T denotes transverse energy, yields equivalent results.

5 Monte Carlo event simulation

Monte Carlo (MC) event samples were employed to model signal and background processes. The generated MC events were passed through the ZEUS detector and trigger simulation programs based on GEANT 3 [39]. They were then reconstructed and analysed using the same programs as used for the data. The effects of the beam-focusing magnet in HERA-II were not well modelled in the ZEUS apparatus simulation.

5.1 RAPGAP

The program RAPGAP 3.2 [3,40] was used to simulate the diffractive process $ep \to ep\gamma X$, where X denotes the presence of final-state hadrons. In addition to enabling acceptance corrections and event-reconstruction efficiencies to be calculated, RAPGAP also provided a physics model to compare to the results of the present measurements. In RAPGAP, the incoming photon is radiated from the electron using the equivalent-photon approximation. The Pomeron carries a fraction $x_{I\!P}$ of the proton longitudinal momentum and is modelled as a hadron-like state within the framework of the factorisation hypothesis of Ingelman and Schlein [4]. In direct photon processes, it is assumed in RAPGAP that the incoming photon scatters elastically off a quark in the resolved Pomeron. In resolved photon processes, gluon–quark and antiquark–quark scattering produce an outgoing photon and a jet. Hadronisation of the outgoing partons is performed using PYTHIA 6.410 [41].

Event samples were generated for direct and resolved photon interactions with a resolved Pomeron. The default parameters were used and the α_s scale was $p^2_{T\,\gamma}$, where $p_{T\,\gamma}$ is the transverse momentum of the outgoing photon. The selected PDF sets were, for the Pomeron, H1 2006 DPDF Fit B [5] and, for the resolved photon, SASGAM-2D [42]. Proton dissociation was not generated in the present analysis. In the original QCD fit by H1 using DIS data [5], resolved Pomeron PDFs were obtained for $z_{I\!P}^{\rm meas} < 0.8$; RAPGAP uses these with an extrapolation to cover the entire $z_{I\!P}^{\rm meas}$ range up to 1.0. Since a simulation of the type of process in Fig. 1(c) was not available, the simulation by RAPGAP was used throughout.

5.2 Background simulations

A background to the isolated photons measured here comes from neutral mesons in hadronic jets, in particular π^0 and η, where meson decay products can create an energy cluster in the BEMC that passes the experimental selection criteria for a photon candidate. To model these effects, RAPGAP was used to generate direct and resolved diffractive scattering that produced exclusive two-jet events that did not contain prompt

photons in the final state. These were analysed using the same program chain as for the prompt photon events.

A separate potential source of background came from non-diffractive prompt photon events; PYTHIA 6.416 was used to generate processes of this type, making use of the CTEQ4 [43] and GRV [44] proton and photon PDF sets.

For additional background studies, Bethe–Heitler (BH) event samples were obtained using the GRAPE-COMPTON MC [45]. DIS event samples with initial-state photon radiation were also generated using the GRAPE-COMPTON and the DJANGOH 6 programs [46] interfaced with ARIADNE [47].

6 Event selection

The basic event selection and reconstruction was performed as previously [17]. A three-level trigger system was used to select events online [28, 48, 49]:

- the first-level trigger required a loosely measured track in the CTD and energy deposited in the CAL that included conditions to select an isolated electromagnetic signal;
- at the second level, conditions for an event with at least 8 GeV of summed transverse energy were imposed;
- at the third level, the event was reconstructed and a high-energy photon candidate was required.

In the offline event analysis, some general conditions were applied as follows:

- to reduce background from non-ep collisions, events were required to have a reconstructed vertex position, $Z_{\rm vtx}$, within the range $|Z_{\rm vtx}| < 40\,{\rm cm}$;
- no identified electron with energy above 3.5 GeV was allowed in the event;
- at least one vertex-fitted track with $p_T > 0.2$ GeV was required;
- the accepted range of incoming virtual photon energies was defined by the requirement $0.2 < y_{\rm JB} < 0.7$. The lower cut strengthened the trigger requirements and the upper cut suppressed DIS events;
- a potential source of unwanted events arises from BH processes of the type $ep \to ep\gamma$, where the outgoing electron is at a wide angle and any possible dissociation products of the proton are not observed in the detector. If collinear initial-state radiation from the beam electron takes place, these events may be recorded within the allowed $y_{\rm JB}$ range, the outgoing electron being interpreted as a jet. Such events have a small number of

outgoing particles in the detector, and are efficiently rejected by the veto on identified electrons, and by a further requirement that the number of energy-flow objects in the event (see below) with energy above 0.2 GeV must exceed 5. The rejection efficiency for these events was close to 100% and was verified by means of event samples from GRAPE-COMPTON that simulated the BH processes. The kinematically similar deeply virtual Compton scattering (DVCS) process was excluded in the same way as the BH processes. Approximately 2% of RAPGAP events were rejected by this selection. The procedure was further checked by a visual scan of the data events.

The event analysis made use of energy-flow objects (EFOs) [50], which were constructed from clusters of calorimeter cells, associated with tracks when appropriate. Tracks not associated with calorimeter clusters were also included. EFOs with no associated track, and with at least 90% of the reconstructed energy measured in the BEMC, were taken as photon candidates. Photon candidates with wider electromagnetic showers than are typical for a single photon were accepted at this stage so as to make possible the evaluation of backgrounds. The photon energy scale was calibrated [17, 51] by means of an analysis of DVCS events recorded by ZEUS, in which the detected final-state particles comprised a scattered electron, whose energy measurement is well understood, and a balancing outgoing photon.

Jet reconstruction was performed making use of all the EFOs in the event, including photon candidates, by means of the k_T clustering algorithm [52] using the E-scheme in the longitudinally invariant inclusive mode [53] with the radius parameter set to 1.0. One of the jets found by this procedure corresponds to or includes the photon candidate. An accompanying jet was used in the analysis; if more than one jet was found, that with the highest transverse energy, $E_T^{\rm jet}$, was selected. In the kinematic region used, the resolution of the jet transverse energy was about 15–20%, estimated using MC simulations.

To reduce the contribution of photons from fragmentation processes, and also the background from the decay of neutral mesons within jets, the photon candidate was required to be isolated from other hadronic activity. This was imposed by requiring that the photon-candidate EFO had at least 90% of the total energy of the reconstructed jet of which it formed a part, a condition that was imposed also in the hadron-level calculations. High-E_T photons radiated from scattered leptons were further suppressed by rejecting photons that had a nearby track. This was achieved by demanding $\Delta R > 0.2$, where

$$\Delta R = \sqrt{(\Delta\phi)^2 + (\Delta\eta)^2} \tag{7}$$

and is the distance to the nearest reconstructed track with momentum greater than 250 MeV in the $\eta - \phi$ plane, where ϕ is the azimuthal angle. This latter condition was applied at the detector level for both MC and for data.

The final event selection was as follows:

- each event was required to contain a photon candidate with a reconstructed transverse energy, E_T^γ, in the range $5 < E_T^\gamma < 15$ GeV and with pseudorapidity, η^γ, in the range $-0.7 < \eta^\gamma < 0.9$;
- a hadronic jet was required to have $E_T^{\rm jet}$ between 4 and 35 GeV and to lie within the pseudorapidity, $\eta^{\rm jet}$, range $-1.5 < \eta^{\rm jet} < 1.8$;
- the maximum pseudorapidity for EFOs with energy above 0.4 GeV, $\eta_{\rm max}$, was required to satisfy $\eta_{\rm max} < 2.5$ in order to select diffractive events, characterised by a large rapidity gap;
- a requirement $x_{I\!P} < 0.03$ was made to reduce further any contamination from non-diffractive events;
- the energy deposited in the FPC was required to be less than 1 GeV for the HERA-I data sample [54].

7 Extraction of the photon signal

The selected samples contain a substantial admixture of background events in which one or more neutral mesons, such as π^0 and η, have decayed to photons, thereby producing a photon candidate in the BEMC. The photon signal was extracted statistically following the approach used in previous ZEUS analyses [17, 25–27]. The method made use of the energy-weighted width, measured in the Z direction, of the BEMC energy cluster comprising the photon candidate. This width was calculated as

$$\langle \delta Z \rangle = \sum_i E_i |Z_i - Z_{\rm cluster}| \,/\, (w_{\rm cell} \sum_i E_i), \tag{8}$$

where Z_i is the Z position of the centre of the i-th cell, $Z_{\rm cluster}$ is the energy-weighted centroid of the EFO cluster, $w_{\rm cell}$ is the width of the cell in the Z direction, and E_i is the energy recorded in the cell. The sum runs over all BEMC cells in the EFO cluster.

The number of isolated-photon events in the data was determined by a binned maximum-likelihood fit to the $\langle \delta Z \rangle$ distribution in the range $0.05 < \langle \delta Z \rangle < 0.8$, varying the relative fractions of the signal and background components as represented by histogram templates obtained from the MC. The fit was performed for each measured cross-section interval, with χ^2 values of typically 1.0 per degree of freedom. Figure 2 shows the fitted $\langle \delta Z \rangle$ distribution for the full sample of selected HERA-II events with a photon candidate and at least one jet. The peak seen at $\langle \delta Z \rangle \sim 0.5$ is due to π^0 decays.

For the HERA-I data sample, starting from 161 (127) selected events containing a photon candidate without (with) at least one accompanying jet, the fit gave 91 (76) photon events.

For the HERA-II data sample, the respective figures were 767 (598) selected events, giving 366±31 (311±28) photon events after the fit. It is apparent that a large fraction of the isolated hard photons are accompanied by one or more observed jets.

8 Event distributions and evaluation of cross sections

After applying the selections described above, event distributions were extracted for the HERA-II data. The distribution of events in $x_\gamma^{\rm meas}$ is shown in Fig. 3. A 70:30 mixture of direct:resolved photon events generated with RAPGAP gives a reasonable description of the data and was employed in the following analysis. This applies both for the full data set and for the two separate ranges of $z_{I\!P}^{\rm meas}$ that are described below.

Figure 4(a) shows the event distribution in $z_{I\!P}^{\rm meas}$, together with the prediction obtained from RAPGAP. RAPGAP describes the distribution well for $z_{I\!P}^{\rm meas} < 0.9$, but above this value the data lie above the RAPGAP prediction. Here, RAPGAP does not simulate all applicable physics processes, such as the type illustrated in Fig. 1(c). A good description of the data is required in order to calculate acceptances; in order to obtain this, a weighting factor of 7.0 may be applied to the direct photon component of RAPGAP for hadron-level values of $z_{I\!P}^{\rm meas}$ above 0.9. The observed $z_{I\!P}^{\rm meas}$ distribution is then well described, and Fig. 4(b) shows that the reweighted RAPGAP also provides better agreement with the $\eta_{\rm max}$ event distribution (see Sections 3 and 6). For the other measured variables, the two RAPGAP descriptions are both good and are generally similar, with no clear discrimination between them. The experimental cross sections were evaluated using acceptances that used the reweighted version of RAPGAP as described above.

A bin-by-bin correction method was used to determine the differential cross section in a given variable, by means of the equation

$$\frac{d\sigma}{dY} = \frac{\mathcal{A}\, N(\gamma)}{\mathcal{L}\, \Delta Y}, \tag{9}$$

where $N(\gamma)$ is the number of photons in a bin as extracted from the $\langle \delta Z \rangle$ fit, ΔY is the bin width, $\mathcal{L}$ is the total integrated luminosity, and $\mathcal{A}$ is a correction given by the reciprocal of the acceptance. The correction $\mathcal{A}$ was calculated, using RAPGAP samples, as the ratio of the number of events that were generated in the given bin, according to the chosen definitions, divided by the number of events obtained in the bin after event reconstruction and selection as for the data. As a check on the bin-by-bin correction method, an expectation-maximisation unfolding technique [55] was applied and gave similar results.

After the background subtraction, it was found that of the events with a photon and at least one jet, approximately 5% of those with $z_{I\!P}^{\rm meas} < 0.9$ had a second accepted jet. The

number of events with a third accepted jet was consistent with zero. No additional jets are expected in events with $z_{I\!P}^{\rm meas} \geq 0.9$, owing to kinematic constraints, and none were found.

9 Systematic uncertainties

The main sources of systematic uncertainty on the measured visible HERA-II cross sections were evaluated as follows:

- the energy of the photon candidate was varied by $\pm 2\%$ in the MC at the detector level, and independently the energy of the accompanying jet was varied by $\pm 2\%$. These variations represent the energy scale uncertainties [51]. Each of them gave variations in the measured cross sections of typically $\pm 5\%$;
- the uncertainty in the acceptance due to the estimation of the relative fractions of direct photon and resolved photon events in the RAPGAP MC sample was estimated by varying the fraction of direct photon events between 60% and 80%; the changes in the cross sections were typically $\pm 2\%$;
- the dependence of the result on the modelling by the MC of the hadronic background in the $\langle \delta Z \rangle$ distribution was investigated by varying the upper limit for the $\langle \delta Z \rangle$ fit in the range $[0.6, 1.0]$ [27]; this gave a $\pm 2\%$ variation;
- the non-diffractive photoproduction background was estimated by fitting a number of experimental variables to mixtures of RAPGAP and PYTHIA samples. The PYTHIA samples were treated in the same way as the data, using an appropriate mixture of resolved and direct photoproduction events. It was found that a satisfactory description of the data was obtained with no non-diffractive background, but that up to 10% of background could not be excluded, as illustrated in Fig. 4. This is included as an asymmetric systematic uncertainty.

The uncertainties listed above were combined in quadrature. The normalisation issues due to proton dissociation as discussed in Section 3 were not further evaluated as they do not affect the shape of the distributions.

A possible contamination of DIS events was investigated using the programs GRAPE-COMPTON and DJANGOH, and a possible contribution arising from photon–photon interactions was investigated using GRAPE-COMPTON. Both of these were found to be negligible. Other sources of systematic uncertainty that were estimated to be negligible included the modelling of the track-isolation cut and the track-momentum cut, and also the cuts on photon isolation, the electromagnetic fraction of the photon shower, $y_{\rm JB}$, and $Z_{\rm vtx}$.

The uncertainties of 2.0% on the trigger efficiency and 1.9% on the luminosity measurement were not included in the figures. These contributions are included in the uncertainties on the visible cross sections determined from the HERA-I data, together with the other systematic uncertainties evaluated as for the HERA-II cross sections.

10 Results

Cross sections were measured for the diffractive production of an isolated photon, inclusive and with at least one accompanying jet, in the kinematic region defined by $Q^2 < 1$ GeV^2, $0.2 < y < 0.7$, $-0.7 < \eta^\gamma < 0.9$, $5 < E_T^\gamma < 15$ GeV, $4 < E_T^{\rm jet} < 35$ GeV and $-1.5 < \eta^{\rm jet} < 1.8$. The diffractive condition required that $\eta_{\rm max} < 2.5$ and $x_{I\!P} < 0.03$. As a result of the removal of the BH and DVCS events, the measurements are sensitive only to events with more than five observed final-state particles, including the isolated photon. This condition was imposed on the MC events at the detector level but not at the hadron level. All cross sections were evaluated at the hadron level in the laboratory frame, and the jets were formed according to the k_T clustering algorithm with the radius parameter set to 1.0. Both at the detector and hadron levels, photon isolation was imposed by requiring that the photon candidate had at least 90% of the total energy of the reconstructed jet of which it formed a part. If more than one accompanying jet was found within the designated $\eta^{\rm jet}$ range in an event, that with highest $E_T^{\rm jet}$ was taken. No subtraction for dissociated-proton states has been made. As explained in Section 3, these are uncertain and could amount to 40% of the visible cross section.

With the above selections, the effect of the $\eta_{\rm max}$ requirement is to remove 64% of the diffractive events with $x_{I\!P} < 0.03$, as evaluated using the RAPGAP model. In order to avoid the large extrapolation that would be needed to include the full $\eta_{\rm max}$ range, and given the additional presence in this range of larger non-diffractive backgrounds and uncertain effects of proton dissociation, "visible" cross sections are quoted here for the range defined by $\eta_{\rm max} < 2.5$ and $x_{I\!P} < 0.03$.

Differential cross sections for inclusive prompt-photon production, using the HERA-II data, are shown for the quantities E_T^γ and η^γ in Fig. 5(a, b). Differential cross sections for the quantities $x_{I\!P}$ and M_X for events with an inclusive prompt photon are shown in Fig. 5(c, d). The predictions of RAPGAP, normalised to the data, are in good agreement with the data in both the unreweighted and reweighted cases. The data are listed in Tables 1–4.

For events containing a photon and at least one jet, the differential cross section as a function of $z_{I\!P}^{\rm meas}$ is plotted in Fig. 6 and listed in Table 5. It shows evidence for an excess of data above the nominal prediction of RAPGAP for $z_{I\!P}^{\rm meas} \geq 0.9$, which lies beyond the

region where the Pomeron PDFs were originally evaluated. As a check on this result, the analysis was repeated with the selection on $\eta_{\max}$ removed and applying different selections on $x_{I\!P}$. These variations had the effect of changing the measured shape of the cross section $d\sigma/dz_{I\!P}^{\rm meas}$ for $z_{I\!P}^{\rm meas} < 0.9$, but the excess above the RAPGAP prediction for $z_{I\!P}^{\rm meas} \geq 0.9$ remained present in each case.

Figures 7–10, together with Tables 6–17, show the differential cross sections for a number of kinematic variables for the full $z_{I\!P}^{\rm meas}$ range and separately for the ranges $z_{I\!P}^{\rm meas} < 0.9$ and $z_{I\!P}^{\rm meas} \geq 0.9$. The variables presented are the transverse energy and the pseudorapidity of the photon and the jet, the incoming photon–proton centre-of-mass energy, W, the ratio of the transverse energies of the photon and the jet, the quantities $x_\gamma^{\rm meas}$, $x_{I\!P}$ and M_X, the differences in azimuth and pseudorapidity of the photon and the jet, $\Delta\phi = |\phi^\gamma - \phi^{\rm jet}|$ and $\Delta\eta = \eta^\gamma - \eta^{\rm jet}$, and $\eta_{\max}$. Cross sections for $E_T^{\rm jet}$ above 15 GeV are omitted from Figs. 8(a)–(c) owing to limited statistics, but the data in this range are included in the other cross-section measurements.

The distributions shown in Figs. 7–10 are generally well described by RAPGAP, apart from $\eta_{\max}$ in Fig. 10(g) when RAPGAP is not reweighted. For $z_{I\!P}^{\rm meas} < 0.9$, RAPGAP normalised to the data in this range is in agreement with the data in all variables. For $z_{I\!P}^{\rm meas} \geq 0.9$, RAPGAP gives a good phenomenological description of the shape of the data. The distribution in $\Delta\phi$ confirms that the data are dominated by events with a photon and one jet. This is also confirmed by the distribution of the ratio of the transverse energies of the photon and the jet.

The cross-section distribution in $z_{I\!P}^{\rm meas}$ may be compared to the results obtained by ZEUS for the diffractive production of dijet systems [12, 54], where the photoproduction data are not well described by RAPGAP but do not show a similar rise at high values of $z_{I\!P}^{\rm meas}$. In DIS, the diffractive production of exclusive dijets was found to be better described by a two-gluon-exchange, or direct Pomeron, model than by RAPGAP [36]. The present prompt-photon results give evidence for the presence of a direct Pomeron process in diffractive photoproduction with $z_{I\!P}^{\rm meas} \geq 0.9$. Events in this region show indications of a resolved photon contribution (Fig. 9(c)), but are dominated by direct photon interactions. This is the first measurement in this channel. At present, no theoretical model is available that might give a quantitative prediction for this effect.

The integrated visible HERA-II cross sections for the diffractive production of a prompt photon in the above kinematic region, inclusively and with at least one jet, are found to be $1.21 \pm 0.10^{+0.10}_{-0.16}$ pb and $1.14 \pm 0.10^{+0.07}_{-0.15}$ pb, respectively. The smaller and calculable proton dissociation contribution in the HERA-I data allows a correction for this effect to be made. Using the HERA-I data, analysed as for the present HERA-II measurements, integrated cross sections of $1.21 \pm 0.19^{+0.14}_{-0.14}$ pb and $1.10 \pm 0.19^{+0.09}_{-0.13}$ pb, respectively, were obtained. These were evaluated with the same event selections and kinematic limits as

for the HERA-II measurements but supplemented by a veto on events with an FPC signal of more than 1 GeV.

The integrated cross section from the HERA-I data, evaluated with the present experimental selections in the range $z_{I\!P}^{\rm meas} < 0.9$, is found to be $0.68 \pm 0.14^{+0.06}_{-0.07}$ pb, with no allowance for proton dissociation. This becomes $0.57 \pm 0.12^{+0.05}_{-0.06}$ pb after multiplying by a dissociation correction factor of 0.84. The corresponding value from RAPGAP is 0.68 pb, with no proton dissociation and no resolved-suppression factor [7, 8]. The agreement in shape and normalisation found with the RAPGAP predictions in the lower $z_{I\!P}^{\rm meas}$ range, obtained using Pomeron PDFs generated from DIS data, is consistent with a common set of Pomeron PDFs in the photoproduction and DIS regimes.

11 Conclusions

The diffractive photoproduction of isolated photons, with and without at least one accompanying jet, has been measured for the first time with the ZEUS detector at HERA, using integrated luminosities of $82 \pm 2\,{\rm pb}^{-1}$ from HERA-I and $374 \pm 7\,{\rm pb}^{-1}$ from HERA-II. Cross sections are presented in a kinematic region defined in the laboratory frame by: $Q^2 < 1$ GeV^2, $0.2 < y < 0.7$, $-0.7 < \eta^\gamma < 0.9$, $5 < E_T^\gamma < 15$ GeV, $4 < E_T^{\rm jet} < 35$ GeV and $-1.5 < \eta^{\rm jet} < 1.8$. The diffractive requirement was $\eta_{\rm max} < 2.5$ and $x_{I\!P} < 0.03$. Photon isolation was imposed by requiring that the photon had at least 90% of the energy of the reconstructed jet of which it formed a part.

Differential cross sections are presented in terms of the transverse energy and pseudorapidity of the prompt photon and the jet, and for a number of variables that describe the kinematic properties of the diffractively produced system, in particular the fraction of the Pomeron energy given to the prompt photon and the jet, $z_{I\!P}^{\rm meas}$.

The data are compared with a standard RAPGAP model that simulates direct and resolved photon interactions with a resolved Pomeron. With the exception of $\eta_{\rm max}$ and $z_{I\!P}^{\rm meas}$, the distributions in all the variables are well described in shape by this model over the whole $z_{I\!P}^{\rm meas}$ range and in the ranges $z_{I\!P}^{\rm meas} < 0.9$ and $z_{I\!P}^{\rm meas} \geq 0.9$ separately. For $z_{I\!P}^{\rm meas} \geq 0.9$, there is evidence for an excess in the data above the nominal RAPGAP prediction. This excess indicates the presence of a direct Pomeron interaction, and is observed predominantly in the direct photon channel.

Acknowledgements

We appreciate the contributions to the construction, maintenance and operation of the ZEUS detector made by many people who are not listed as authors. The HERA machine group and the DESY computing staff are especially acknowledged for their success in providing excellent operation of the collider and the data-analysis environment. We thank the DESY directorate for their strong support and encouragement. We also thank H. Jung for providing invaluable assistance with the use of RAPGAP.

References

[1] G. Watt, A.D. Martin and M.G. Ryskin, arXiv:0708.4126;
A. Martin, M. Ryskin and G. Watt, Phys. Lett. B 644 (2007) 131.

[2] M. Wüsthoff, Ph.D Thesis, DESY-95-166 (1995);
M. Diehl, Z. Phys. C76 (1997) 499;
J. Bartels et al., in Proc. *Workshop on Future Physics at HERA,* eds. A. De Roeck, G. Ingelman and R. Klanner, DESY (1995/966) 668, hep-ph/9609239.

[3] H. Jung, https://rapgap.hepforge.org/rapgap.pdf.

[4] G. Ingelman and P. Schlein, Phys. Lett. B 152 (1985) 256.

[5] H1 Collaboration, A. Aktas et al., Eur. Phys. J. C 48 (2006) 715.

[6] B. Kniehl, H.-G. Kohrs and G. Kramer, Z. Phys. C 65 (1995) 657;
H.-G. Kohrs, hep-ph/9507208;
A. Donnachie and P.V. Landshoff, Phys. Lett. B 285 (1992) 172.

[7] J. Collins, Phys. Rev. D 57 (1998) 3051, erratum Phys. Rev. D 61 (2000) 019902.

[8] A. Kaidalov et al., Eur. Phys. J. C 21 (2001) 521.

[9] M. Klasen and G. Kramer, in Proc. *12 International Workshop on Deep Inelastic Scattering,* eds. D. Bruncko, J. Ferencei and P. Striženeć (2004) 492, hep-ph/0401202.

[10] H1 Collaboration, F.D. Aaron et al., Eur. Phys. J. C 70 (2010) 15.

[11] H1 Collaboration, C. Adloff et al., Eur. Phys. J. C 6 (1999) 421.

[12] ZEUS Collaboration, S. Chekanov et al., Eur. Phys. J. C 55 (2008) 177.

[13] H1 Collaboration, V. Andreev et al., JHEP 1505 (2015) 056.

[14] ZEUS Collaboration, J. Breitweg et al., Eur. Phys. J. C 5 (1998) 41.

[15] H1 Collaboration, A. Aktas et al., Eur. Phys. J. C 51 (2007) 549.

[16] H1 Collaboration, V. Andreev et al., Phys. Lett. B 672 (2009) 219.

[17] ZEUS Collaboration, H. Abramowicz et al., Phys. Lett. B 730 (2014) 293.

[18] ZEUS Collaboration, J. Breitweg et al., Phys. Lett. B 413 (1997) 201.

[19] ZEUS Collaboration, J. Breitweg et al., Phys. Lett. B 472 (2000) 175.

[20] ZEUS Collaboration, S. Chekanov et al., Phys. Lett. B 511 (2001) 19.

[21] ZEUS Collaboration, S. Chekanov et al., Eur. Phys. J. C 49 (2007) 511.

[22] H1 Collaboration, A. Aktas et al., Eur. Phys. J. C 38 (2004) 437.

[23] H1 Collaboration, F.D. Aaron et al., Eur. Phys. J. C 66 (2010) 17.

[24] H1 Collaboration, F.D. Aaron et al., Eur. Phys. J. C 54 (2008) 371.

[25] ZEUS Collaboration, S. Chekanov et al., Phys. Lett. B 595 (2004) 86.

[26] ZEUS Collaboration, S. Chekanov et al., Phys. Lett. B 687 (2010) 16.

[27] ZEUS Collaboration, H. Abramowicz et al., Phys. Lett. B 715 (2012) 88.

[28] ZEUS Collaboration, U. Holm (ed.), *The ZEUS Detector*. Status Report (unpublished), DESY (1993), available on `http://www-zeus.desy.de/bluebook/bluebook.html`.

[29] N. Harnew et al., Nucl. Inst. Meth. A 279 (1989) 290;
B. Foster et al., Nucl. Phys. Proc. Suppl. B 32 (1993) 181;
B. Foster et al., Nucl. Inst. Meth. A 338 (1994) 254.

[30] A. Polini et al., Nucl. Inst. Meth. A 581 (2007) 656.

[31] M. Derrick et al., Nucl. Inst. Meth. A 309 (1991) 77;
A. Andresen et al., Nucl. Inst. Meth. A 309 (1991) 101;
A. Caldwell et al., Nucl. Inst. Meth. A 321 (1992) 356;
A. Bernstein et al., Nucl. Inst. Meth. A 336 (1993) 23.

[32] A. Bamburger et al., Nucl. Inst. Meth. A 450 (2000) 235.

[33] L. Adamczyk et al., Nucl. Inst. Meth. A 744 (2014) 80.

[34] J. Andruszków et al., Preprint DESY-92-066, DESY, 1992;
ZEUS Collaboration, M. Derrick et al., Z. Phys. C 63 (1994) 391;
J. Andruszków et al., Acta Phys. Pol. B 32 (2001) 2025.

[35] M. Helbich et al., Nucl. Inst. Meth. A 565 (2006) 572.

[36] ZEUS Collaboration, H. Abramowicz et al., Eur. Phys. J. C 76 (2016) 1.

[37] F. Jacquet and A. Blondel, Proc. *Study for an ep Facility for Europe,* DESY 79/48 (1979) 391.

[38] ZEUS Collaboration, M. Derrick et al., Phys. Lett. B 303 (1993) 183.

[39] R. Brun et al., GEANT3, Technical Report CERN-DD/EE/84-1, CERN (1987).

[40] H. Jung, private communication.

[41] T. Sjöstrand et al., JHEP 05 (2006) 26.

[42] G. Schuler and T. Sjöstrand, Phys. Lett. B 376 (1996) 193.

[43] H.L. Lai et al., Phys. Rev. D 55 (1997) 1280.

[44] M. Glück, G. Reya and A. Vogt, Phys. Rev. D 45 (1992) 3986;
M. Glück, G. Reya and A. Vogt, Phys. Rev. D 46 (1992) 1973.

[45] T. Abe, Comp. Phys. Comm. 136 (2001) 126.

[46] H. Spiesberger, *HERACLES and DJANGOH Event Generators for ep Interactions at HERA Including Radiative Processes,* 1998, `http://wwwthep.physik.uni-mainz.de/~hspiesb/djangoh/djangoh.html`.

[47] L. Lönnblad, Comp. Phys. Comm. 71 (1992) 15;
L. Lönnblad, Z. Phys. C 65 (1995) 285.

[48] W.H. Smith, K. Tokushuku and L.W. Wiggers, *Proc. Computing in High-Energy Physics (CHEP), Annecy, France, Sep. 1992*, eds. C. Verkerk and W. Wojcik, CERN, Geneva, Switzerland (1992) 222. Also in preprint DESY 92-150B.

[49] P. Allfrey et al., Nucl. Inst. Meth. A 580 (2007) 1257.

[50] ZEUS Collaboration, J. Breitweg et al., Eur. Phys. J. C 1 (1998) 81;
ZEUS Collaboration, J. Breitweg et al., Eur. Phys. J. C 6 (1999) 43.

[51] A. Iudin, Ph.D. Thesis, Kyiv National University "Kyiv Polytechnic Institute" (2014, unpublished).

[52] S. Catani et al., Nucl. Phys. B 406 (1993) 187.

[53] S.D. Ellis and D.E. Soper, Phys. Rev. D 48 (1993) 3160.

[54] S. Kagawa, Ph.D. thesis, KEK Report 2005-12 (2006).

[55] G. D'Agostini, Nucl. Instr. Meth. A 362 (1995) 487;
G. Kondor, Nucl. Instr. Meth. A 216 (1983) 177;
H. Mülthei and B. Schorr, Nucl. Instr. Meth. A 257 (1987) 371.

E_T^γ range (GeV)	$\frac{d\sigma}{dE_T^\gamma}$ (pb GeV^{-1})
5.0 – 6.0	$0.549 \pm 0.087\,(\text{stat.})\,^{+0.033}_{-0.072}\,(\text{syst.})$
6.0 – 7.0	$0.269 \pm 0.054\,(\text{stat.})\,^{+0.038}_{-0.038}\,(\text{syst.})$
7.0 – 8.0	$0.187 \pm 0.032\,(\text{stat.})\,^{+0.023}_{-0.027}\,(\text{syst.})$
8.0 – 15.0	$0.031 \pm 0.005\,(\text{stat.})\,^{+0.004}_{-0.005}\,(\text{syst.})$

Table 1: *Differential cross-section $\frac{d\sigma}{dE_T^\gamma}$ for inclusive photons in diffractive photoproduction. (Figure 5(a))*

η^γ range	$\frac{d\sigma}{d\eta^\gamma}$ (pb)
−0.7 – −0.3	$1.33 \pm 0.19\,(\text{stat.})\,^{+0.13}_{-0.18}\,(\text{syst.})$
−0.3 – 0.1	$0.87 \pm 0.14\,(\text{stat.})\,^{+0.09}_{-0.11}\,(\text{syst.})$
0.1 – 0.5	$0.419 \pm 0.105\,(\text{stat.})\,^{+0.019}_{-0.057}\,(\text{syst.})$
0.5 – 0.9	$0.485 \pm 0.095\,(\text{stat.})\,^{+0.056}_{-0.064}\,(\text{syst.})$

Table 2: *Differential cross-section $\frac{d\sigma}{d\eta^\gamma}$ for inclusive photons in diffractive photoproduction. (Figure 5(b))*

$x_{I\!P}$ range	$\frac{d\sigma}{dx_{I\!P}}$ (pb)
0.0 – 0.005	$24.3 \pm 7.5\,(\text{stat.})\,^{+2.0}_{-3.9}\,(\text{syst.})$
0.005 – 0.01	$87.6 \pm 12.8\,(\text{stat.})\,^{+7.8}_{-11.1}\,(\text{syst.})$
0.01 – 0.015	$67.1 \pm 10.9\,(\text{stat.})\,^{+5.5}_{-11.0}\,(\text{syst.})$
0.015 – 0.02	$41.9 \pm 8.6\,(\text{stat.})\,^{+3.3}_{-5.8}\,(\text{syst.})$
0.02 – 0.025	$15.4 \pm 4.7\,(\text{stat.})\,^{+1.3}_{-2.0}\,(\text{syst.})$
0.025 – 0.03	$4.9 \pm 3.2\,(\text{stat.})\,^{+1.5}_{-0.9}\,(\text{syst.})$

Table 3: *Differential cross-section $\frac{d\sigma}{dx_{I\!P}}$ for inclusive photons in diffractive photoproduction.(Figure 5(c))*

M_X range (GeV)	$\frac{d\sigma}{dM_X}$ (pb GeV^{-1})
10.0 – 15.0	$0.048 \pm 0.008\,(\text{stat.})\,^{+0.006}_{-0.006}\,(\text{syst.})$
15.0 – 20.0	$0.101 \pm 0.014\,(\text{stat.})\,^{+0.010}_{-0.015}\,(\text{syst.})$
20.0 – 25.0	$0.053 \pm 0.009\,(\text{stat.})\,^{+0.010}_{-0.009}\,(\text{syst.})$
25.0 – 30.0	$0.029 \pm 0.007\,(\text{stat.})\,^{+0.002}_{-0.005}\,(\text{syst.})$
30.0 – 40.0	$0.005 \pm 0.002\,(\text{stat.})\,^{+0.001}_{-0.001}\,(\text{syst.})$

Table 4: *Differential cross-section $\frac{d\sigma}{dM_X}$ for inclusive photons in diffractive photoproduction. (Figure 5(d))*

$z_{I\!P}^{\text{meas}}$ range	$\frac{d\sigma}{dz_{I\!P}^{\text{meas}}}$ (pb)
0.0 – 0.4	$0.25 \pm 0.08\,(\text{stat.})\,^{+0.01}_{-0.04}\,(\text{syst.})$
0.4 – 0.5	$0.74 \pm 0.29\,(\text{stat.})\,^{+0.10}_{-0.15}\,(\text{syst.})$
0.5 – 0.6	$1.12 \pm 0.32\,(\text{stat.})\,^{+0.05}_{-0.14}\,(\text{syst.})$
0.6 – 0.7	$1.73 \pm 0.35\,(\text{stat.})\,^{+0.12}_{-0.24}\,(\text{syst.})$
0.7 – 0.8	$1.44 \pm 0.29\,(\text{stat.})\,^{+0.15}_{-0.15}\,(\text{syst.})$
0.8 – 0.9	$1.02 \pm 0.27\,(\text{stat.})\,^{+0.13}_{-0.19}\,(\text{syst.})$
0.9 – 1.0	$4.79 \pm 0.65\,(\text{stat.})\,^{+0.83}_{-0.93}\,(\text{syst.})$

Table 5: *Differential cross-section $\frac{d\sigma}{dz_{I\!P}^{\text{meas}}}$ for photons accompanied by at least one jet in diffractive photoproduction. (Figure 6)*

E_T^γ range (GeV)	$\frac{d\sigma}{dE_T^\gamma}$ (pb GeV^{-1})
$0 < z_{I\!P}^{\rm meas} \leq 1.0$	
5.0 – 6.0	$0.483 \pm 0.081\,(\text{stat.})\,^{+0.021}_{-0.067}\,(\text{syst.})$
6.0 – 7.0	$0.257 \pm 0.052\,(\text{stat.})\,^{+0.024}_{-0.030}\,(\text{syst.})$
7.0 – 8.0	$0.185 \pm 0.033\,(\text{stat.})\,^{+0.025}_{-0.026}\,(\text{syst.})$
8.0 – 15.0	$0.031 \pm 0.005\,(\text{stat.})\,^{+0.004}_{-0.004}\,(\text{syst.})$
$z_{I\!P}^{\rm meas} < 0.9$	
5.0 – 6.0	$0.314 \pm 0.052\,(\text{stat.})\,^{+0.009}_{-0.040}\,(\text{syst.})$
6.0 – 7.0	$0.143 \pm 0.034\,(\text{stat.})\,^{+0.015}_{-0.016}\,(\text{syst.})$
7.0 – 8.0	$0.122 \pm 0.026\,(\text{stat.})\,^{+0.012}_{-0.015}\,(\text{syst.})$
8.0 – 15.0	$0.014 \pm 0.003\,(\text{stat.})\,^{+0.001}_{-0.002}\,(\text{syst.})$
$z_{I\!P}^{\rm meas} \geq 0.9$	
5.0 – 6.0	$0.112 \pm 0.044\,(\text{stat.})\,^{+0.023}_{-0.029}\,(\text{syst.})$
6.0 – 7.0	$0.118 \pm 0.035\,(\text{stat.})\,^{+0.025}_{-0.023}\,(\text{syst.})$
7.0 – 8.0	$0.056 \pm 0.018\,(\text{stat.})\,^{+0.017}_{-0.014}\,(\text{syst.})$
8.0 – 15.0	$0.015 \pm 0.003\,(\text{stat.})\,^{+0.003}_{-0.002}\,(\text{syst.})$

Table 6: *Differential cross-section $\frac{d\sigma}{dE_T^\gamma}$ for photons accompanied by at least one jet in diffractive photoproduction. Here and below, the differences between the results evaluated for the entire $z_{I\!P}^{\rm meas}$ range and the sum of the corresponding results for the two partial ranges are of statistical origin. (Figure 7(a–c))*

η^γ range	$\frac{d\sigma}{d\eta^\gamma}$ (pb)
$0 < z_{I\!P}^{\rm meas} \leq 1.0$	
-0.7 – -0.3	$1.24 \pm 0.18\,(\text{stat.})\,^{+0.08}_{-0.16}\,(\text{syst.})$
-0.3 – 0.1	$0.78 \pm 0.13\,(\text{stat.})\,^{+0.06}_{-0.10}\,(\text{syst.})$
0.1 – 0.5	$0.46 \pm 0.11\,(\text{stat.})\,^{+0.02}_{-0.06}\,(\text{syst.})$
0.5 – 0.9	$0.45 \pm 0.09\,(\text{stat.})\,^{+0.04}_{-0.07}\,(\text{syst.})$
$z_{I\!P}^{\rm meas} < 0.9$	
-0.7 – -0.3	$0.70 \pm 0.11\,(\text{stat.})\,^{+0.04}_{-0.08}\,(\text{syst.})$
-0.3 – 0.1	$0.47 \pm 0.09\,(\text{stat.})\,^{+0.04}_{-0.06}\,(\text{syst.})$
0.1 – 0.5	$0.28 \pm 0.07\,(\text{stat.})\,^{+0.02}_{-0.03}\,(\text{syst.})$
0.5 – 0.9	$0.26 \pm 0.07\,(\text{stat.})\,^{+0.02}_{-0.04}\,(\text{syst.})$
$z_{I\!P}^{\rm meas} \geq 0.9$	
-0.7 – -0.3	$0.44 \pm 0.11\,(\text{stat.})\,^{+0.11}_{-0.09}\,(\text{syst.})$
-0.3 – 0.1	$0.29 \pm 0.09\,(\text{stat.})\,^{+0.07}_{-0.06}\,(\text{syst.})$
0.1 – 0.5	$0.21 \pm 0.07\,(\text{stat.})\,^{+0.04}_{-0.05}\,(\text{syst.})$
0.5 – 0.9	$0.19 \pm 0.07\,(\text{stat.})\,^{+0.03}_{-0.05}\,(\text{syst.})$

Table 7: *Differential cross-section $\frac{d\sigma}{d\eta^\gamma}$ for photons accompanied by at least one jet in diffractive photoproduction. (Figure 7(d–f))*

W range (GeV)	$\frac{d\sigma}{dW}$ (pb GeV^{-1})
$0 < z_{I\!P}^{\rm meas} \leq 1.0$	
140 – 160	$0.0089 \pm 0.0020\,(\text{stat.})\,^{+0.0005}_{-0.0012}\,(\text{syst.})$
160 – 180	$0.0163 \pm 0.0027\,(\text{stat.})\,^{+0.0013}_{-0.0023}\,(\text{syst.})$
180 – 200	$0.0121 \pm 0.0023\,(\text{stat.})\,^{+0.0007}_{-0.0015}\,(\text{syst.})$
200 – 220	$0.0102 \pm 0.0024\,(\text{stat.})\,^{+0.0008}_{-0.0012}\,(\text{syst.})$
220 – 240	$0.0059 \pm 0.0015\,(\text{stat.})\,^{+0.0005}_{-0.0007}\,(\text{syst.})$
240 – 260	$0.0050 \pm 0.0015\,(\text{stat.})\,^{+0.0002}_{-0.0006}\,(\text{syst.})$
$z_{I\!P}^{\rm meas} < 0.9$	
140 – 160	$0.0045 \pm 0.0012\,(\text{stat.})\,^{+0.0002}_{-0.0005}\,(\text{syst.})$
160 – 180	$0.0086 \pm 0.0016\,(\text{stat.})\,^{+0.0003}_{-0.0012}\,(\text{syst.})$
180 – 200	$0.0079 \pm 0.0016\,(\text{stat.})\,^{+0.0004}_{-0.0009}\,(\text{syst.})$
200 – 220	$0.0054 \pm 0.0015\,(\text{stat.})\,^{+0.0003}_{-0.0006}\,(\text{syst.})$
220 – 240	$0.0044 \pm 0.0013\,(\text{stat.})\,^{+0.0003}_{-0.0005}\,(\text{syst.})$
240 – 260	$0.0032 \pm 0.0013\,(\text{stat.})\,^{+0.0003}_{-0.0004}\,(\text{syst.})$
$z_{I\!P}^{\rm meas} \geq 0.9$	
140 – 160	$0.0042 \pm 0.0016\,(\text{stat.})\,^{+0.0002}_{-0.0008}\,(\text{syst.})$
160 – 180	$0.0062 \pm 0.0016\,(\text{stat.})\,^{+0.0010}_{-0.0010}\,(\text{syst.})$
180 – 200	$0.0031 \pm 0.0013\,(\text{stat.})\,^{+0.0012}_{-0.0007}\,(\text{syst.})$
200 – 220	$0.0047 \pm 0.0017\,(\text{stat.})\,^{+0.0015}_{-0.0012}\,(\text{syst.})$
220 – 240	$0.0015 \pm 0.0008\,(\text{stat.})\,^{+0.0005}_{-0.0004}\,(\text{syst.})$
240 – 260	$0.0015 \pm 0.0007\,(\text{stat.})\,^{+0.0003}_{-0.0004}\,(\text{syst.})$

Table 8: *Differential cross-section $\frac{d\sigma}{dW}$ for photons accompanied by at least one jet in diffractive photoproduction. (Figure 7(g–i))*

$E_T^{\rm jet}$ range (GeV)	$\frac{d\sigma}{dE_T^{\rm jet}}$ (pb GeV^{-1})
$0 < z_{I\!P}^{\rm meas} \leq 1.0$	
4.0 – 6.0	$0.178 \pm 0.032\,(\text{stat.})\,^{+0.011}_{-0.029}\,(\text{syst.})$
6.0 – 8.0	$0.253 \pm 0.036\,(\text{stat.})\,^{+0.023}_{-0.030}\,(\text{syst.})$
8.0 – 10.0	$0.112 \pm 0.019\,(\text{stat.})\,^{+0.007}_{-0.015}\,(\text{syst.})$
10.0 – 15.0	$0.016 \pm 0.004\,(\text{stat.})\,^{+0.003}_{-0.002}\,(\text{syst.})$
$z_{I\!P}^{\rm meas} < 0.9$	
4.0 – 6.0	$0.136 \pm 0.025\,(\text{stat.})\,^{+0.007}_{-0.020}\,(\text{syst.})$
6.0 – 8.0	$0.128 \pm 0.022\,(\text{stat.})\,^{+0.016}_{-0.015}\,(\text{syst.})$
8.0 – 10.0	$0.061 \pm 0.012\,(\text{stat.})\,^{+0.003}_{-0.006}\,(\text{syst.})$
10.0 – 15.0	$0.006 \pm 0.002\,(\text{stat.})\,^{+0.001}_{-0.001}\,(\text{syst.})$
$z_{I\!P}^{\rm meas} \geq 0.9$	
4.0 – 6.0	$0.030 \pm 0.013\,(\text{stat.})\,^{+0.010}_{-0.007}\,(\text{syst.})$
6.0 – 8.0	$0.126 \pm 0.026\,(\text{stat.})\,^{+0.024}_{-0.024}\,(\text{syst.})$
8.0 – 10.0	$0.043 \pm 0.013\,(\text{stat.})\,^{+0.006}_{-0.010}\,(\text{syst.})$
10.0 – 15.0	$0.010 \pm 0.003\,(\text{stat.})\,^{+0.002}_{-0.002}\,(\text{syst.})$

Table 9: *Differential cross-section $\frac{d\sigma}{dE_T^{\rm jet}}$ for photons accompanied by at least one jet in diffractive photoproduction. (Figure 8(a–c))*

$\eta^{\rm jet}$ range	$\frac{d\sigma}{d\eta^{\rm jet}}$ (pb)
$0 < z_{I\!P}^{\rm meas} \leq 1.0$	
-1.5 – -0.7	$0.38 \pm 0.06\,(\text{stat.})\,^{+0.03}_{-0.05}\,(\text{syst.})$
-0.7 – 0.1	$0.53 \pm 0.08\,(\text{stat.})\,^{+0.04}_{-0.06}\,(\text{syst.})$
0.1 – 0.9	$0.43 \pm 0.07\,(\text{stat.})\,^{+0.02}_{-0.07}\,(\text{syst.})$
0.9 – 1.8	$0.09 \pm 0.03\,(\text{stat.})\,^{+0.00}_{-0.01}\,(\text{syst.})$
$z_{I\!P}^{\rm meas} < 0.9$	
-1.5 – -0.7	$0.27 \pm 0.05\,(\text{stat.})\,^{+0.02}_{-0.03}\,(\text{syst.})$
-0.7 – 0.1	$0.32 \pm 0.05\,(\text{stat.})\,^{+0.02}_{-0.03}\,(\text{syst.})$
0.1 – 0.9	$0.24 \pm 0.05\,(\text{stat.})\,^{+0.01}_{-0.04}\,(\text{syst.})$
0.9 – 1.8	$0.03 \pm 0.02\,(\text{stat.})\,^{+0.01}_{-0.01}\,(\text{syst.})$
$z_{I\!P}^{\rm meas} \geq 0.9$	
-1.5 – -0.7	$0.08 \pm 0.03\,(\text{stat.})\,^{+0.03}_{-0.02}\,(\text{syst.})$
-0.7 – 0.1	$0.18 \pm 0.05\,(\text{stat.})\,^{+0.04}_{-0.04}\,(\text{syst.})$
0.1 – 0.9	$0.17 \pm 0.04\,(\text{stat.})\,^{+0.03}_{-0.04}\,(\text{syst.})$
0.9 – 1.8	$0.09 \pm 0.03\,(\text{stat.})\,^{+0.03}_{-0.02}\,(\text{syst.})$

Table 10: *Differential cross-section $\frac{d\sigma}{d\eta^{\rm jet}}$ for photons accompanied by at least one jet in diffractive photoproduction. (Figure 8(d–f))*

$E_T^\gamma/E_T^{\rm jet}$ range	$\frac{d\sigma}{d(E_T^\gamma/E_T^{\rm jet})}$ (pb)
$0 < z_{I\!P}^{\rm meas} \leq 1.0$	
0.4 – 0.6	$0.012 \pm 0.007\,(\text{stat.})\,^{+0.005}_{-0.002}\,(\text{syst.})$
0.6 – 0.8	$0.62 \pm 0.13\,(\text{stat.})\,^{+0.08}_{-0.15}\,(\text{syst.})$
0.8 – 1.0	$2.68 \pm 0.45\,(\text{stat.})\,^{+0.43}_{-0.30}\,(\text{syst.})$
1.0 – 1.2	$1.29 \pm 0.24\,(\text{stat.})\,^{+0.13}_{-0.20}\,(\text{syst.})$
1.2 – 1.4	$0.35 \pm 0.09\,(\text{stat.})\,^{+0.11}_{-0.09}\,(\text{syst.})$
1.4 – 1.6	$0.15 \pm 0.05\,(\text{stat.})\,^{+0.05}_{-0.03}\,(\text{syst.})$
$z_{I\!P}^{\rm meas} < 0.9$	
0.4 – 0.6	$0.010 \pm 0.006\,(\text{stat.})\,^{+0.005}_{-0.002}\,(\text{syst.})$
0.6 – 0.8	$0.36 \pm 0.10\,(\text{stat.})\,^{+0.05}_{-0.08}\,(\text{syst.})$
0.8 – 1.0	$1.28 \pm 0.27\,(\text{stat.})\,^{+0.24}_{-0.20}\,(\text{syst.})$
1.0 – 1.2	$0.95 \pm 0.22\,(\text{stat.})\,^{+0.07}_{-0.17}\,(\text{syst.})$
1.2 – 1.4	$0.31 \pm 0.09\,(\text{stat.})\,^{+0.08}_{-0.07}\,(\text{syst.})$
1.4 – 1.6	$0.15 \pm 0.05\,(\text{stat.})\,^{+0.05}_{-0.02}\,(\text{syst.})$
$z_{I\!P}^{\rm meas} \geq 0.9$	
0.6 – 0.8	$0.24 \pm 0.08\,(\text{stat.})\,^{+0.07}_{-0.07}\,(\text{syst.})$
0.8 – 1.0	$1.19 \pm 0.29\,(\text{stat.})\,^{+0.27}_{-0.16}\,(\text{syst.})$
1.0 – 1.2	$0.33 \pm 0.09\,(\text{stat.})\,^{+0.16}_{-0.06}\,(\text{syst.})$

Table 11: *Differential cross-section $\frac{d\sigma}{d(E_T^\gamma/E_T^{\rm jet})}$ for photons accompanied by at least one jet in diffractive photoproduction. Omitted values for $z_{I\!P}^{\rm meas} \geq 0.9$ are consistent with zero. (Figure 8(g–i))*

$x_\gamma^{\rm meas}$ range	$\frac{d\sigma}{dx_\gamma^{\rm meas}}$ (pb)
$0 < z_{I\!P}^{\rm meas} \leq 1.0$	
0.1 – 0.6	$0.16 \pm 0.08\,(\text{stat.})\,^{+0.03}_{-0.05}\,(\text{syst.})$
0.6 – 0.7	$0.54 \pm 0.20\,(\text{stat.})\,^{+0.09}_{-0.11}\,(\text{syst.})$
0.7 – 0.8	$1.25 \pm 0.31\,(\text{stat.})\,^{+0.09}_{-0.20}\,(\text{syst.})$
0.8 – 0.9	$1.95 \pm 0.35\,(\text{stat.})\,^{+0.18}_{-0.20}\,(\text{syst.})$
0.9 – 1.0	$5.98 \pm 0.64\,(\text{stat.})\,^{+0.50}_{-0.81}\,(\text{syst.})$
$z_{I\!P}^{\rm meas} < 0.9$	
0.1 – 0.6	$0.08 \pm 0.07\,(\text{stat.})\,^{+0.04}_{-0.04}\,(\text{syst.})$
0.6 – 0.7	$0.49 \pm 0.18\,(\text{stat.})\,^{+0.05}_{-0.10}\,(\text{syst.})$
0.7 – 0.8	$1.01 \pm 0.27\,(\text{stat.})\,^{+0.07}_{-0.16}\,(\text{syst.})$
0.8 – 0.9	$1.80 \pm 0.34\,(\text{stat.})\,^{+0.27}_{-0.21}\,(\text{syst.})$
0.9 – 1.0	$2.81 \pm 0.37\,(\text{stat.})\,^{+0.09}_{-0.30}\,(\text{syst.})$
$z_{I\!P}^{\rm meas} \geq 0.9$	
0.1 – 0.6	$0.11 \pm 0.05\,(\text{stat.})\,^{+0.02}_{-0.05}\,(\text{syst.})$
0.6 – 0.7	$0.08 \pm 0.07\,(\text{stat.})\,^{+0.05}_{-0.02}\,(\text{syst.})$
0.7 – 0.8	$0.21 \pm 0.16\,(\text{stat.})\,^{+0.03}_{-0.04}\,(\text{syst.})$
0.8 – 0.9	$0.26 \pm 0.13\,(\text{stat.})\,^{+0.06}_{-0.07}\,(\text{syst.})$
0.9 – 1.0	$2.78 \pm 0.48\,(\text{stat.})\,^{+0.57}_{-0.54}\,(\text{syst.})$

Table 12: *Differential cross-section $\frac{d\sigma}{dx_\gamma^{\rm meas}}$ for photons accompanied by at least one jet in diffractive photoproduction. (Figure 9(a–c))*

$x_{I\!P}$ range	$\frac{d\sigma}{dx_{I\!P}}$ (pb)
$0 < z_{I\!P}^{\rm meas} \leq 1.0$	
0.0 – 0.005	$26.0 \pm 7.0\,(\text{stat.})\,^{+3.3}_{-3.1}\,(\text{syst.})$
0.005 – 0.01	$76.4 \pm 11.8\,(\text{stat.})\,^{+5.6}_{-9.1}\,(\text{syst.})$
0.01 – 0.015	$70.6 \pm 10.2\,(\text{stat.})\,^{+3.2}_{-11.0}\,(\text{syst.})$
0.015 – 0.02	$37.8 \pm 7.9\,(\text{stat.})\,^{+2.6}_{-4.8}\,(\text{syst.})$
0.02 – 0.025	$11.7 \pm 4.1\,(\text{stat.})\,^{+0.8}_{-1.4}\,(\text{syst.})$
0.025 – 0.03	$5.4 \pm 3.3\,(\text{stat.})\,^{+2.0}_{-0.6}\,(\text{syst.})$
$z_{I\!P}^{\rm meas} < 0.9$	
0.0 – 0.005	$9.0 \pm 3.0\,(\text{stat.})\,^{+4.3}_{-1.5}\,(\text{syst.})$
0.005 – 0.01	$40.4 \pm 7.5\,(\text{stat.})\,^{+3.7}_{-4.5}\,(\text{syst.})$
0.01 – 0.015	$49.8 \pm 8.5\,(\text{stat.})\,^{+1.4}_{-7.8}\,(\text{syst.})$
0.015 – 0.02	$26.6 \pm 6.5\,(\text{stat.})\,^{+1.4}_{-3.4}\,(\text{syst.})$
0.02 – 0.025	$9.5 \pm 3.6\,(\text{stat.})\,^{+0.7}_{-1.2}\,(\text{syst.})$
0.025 – .0.03	$2.3 \pm 2.0\,(\text{stat.})\,^{+1.1}_{-0.2}\,(\text{syst.})$
$z_{I\!P}^{\rm meas} \geq 0.9$	
0.0 – 0.005	$11.6 \pm 5.5\,(\text{stat.})\,^{+4.7}_{-3.6}\,(\text{syst.})$
0.005 – 0.01	$31.9 \pm 8.9\,(\text{stat.})\,^{+9.2}_{-7.1}\,(\text{syst.})$
0.01 – 0.015	$20.8 \pm 5.0\,(\text{stat.})\,^{+4.0}_{-4.8}\,(\text{syst.})$
0.015 – 0.02	$10.6 \pm 3.7\,(\text{stat.})\,^{+1.9}_{-1.7}\,(\text{syst.})$
0.02 – 0.025	$3.1 \pm 3.3\,(\text{stat.})\,^{+0.4}_{-0.8}\,(\text{syst.})$
0.025 – 0.03	$9.5 \pm 10.5\,(\text{stat.})\,^{+2.3}_{-4.7}\,(\text{syst.})$

Table 13: *Differential cross-section $\frac{d\sigma}{dx_{I\!P}}$ for photons accompanied by at least one jet in diffractive photoproduction. (Figure 9(d–f))*

M_X range (GeV)	$\frac{d\sigma}{dM_X}$ (pb GeV^{-1})
$0 < z_{I\!P}^{\rm meas} \leq 1.0$	
10.0 – 15.0	$0.042 \pm 0.008\,(\text{stat.})\,^{+0.003}_{-0.005}\,(\text{syst.})$
15.0 – 20.0	$0.091 \pm 0.012\,(\text{stat.})\,^{+0.007}_{-0.013}\,(\text{syst.})$
20.0 – 25.0	$0.055 \pm 0.009\,(\text{stat.})\,^{+0.007}_{-0.009}\,(\text{syst.})$
25.0 – 30.0	$0.029 \pm 0.006\,(\text{stat.})\,^{+0.001}_{-0.004}\,(\text{syst.})$
30.0 – 40.0	$0.004 \pm 0.002\,(\text{stat.})\,^{+0.001}_{-0.000}\,(\text{syst.})$
$z_{I\!P}^{\rm meas} < 0.9$	
10.0 – 15.0	$0.013 \pm 0.003\,(\text{stat.})\,^{+0.003}_{-0.002}\,(\text{syst.})$
15.0 – 20.0	$0.051 \pm 0.009\,(\text{stat.})\,^{+0.003}_{-0.007}\,(\text{syst.})$
20.0 – 25.0	$0.042 \pm 0.008\,(\text{stat.})\,^{+0.007}_{-0.007}\,(\text{syst.})$
25.0 – 30.0	$0.024 \pm 0.006\,(\text{stat.})\,^{+0.001}_{-0.004}\,(\text{syst.})$
30.0 – 40.0	$0.003 \pm 0.002\,(\text{stat.})\,^{+0.001}_{-0.000}\,(\text{syst.})$
$z_{I\!P}^{\rm meas} \geq 0.9$	
10.0 – 15.0	$0.024 \pm 0.007\,(\text{stat.})\,^{+0.004}_{-0.005}\,(\text{syst.})$
15.0 – 20.0	$0.039 \pm 0.008\,(\text{stat.})\,^{+0.008}_{-0.009}\,(\text{syst.})$
20.0 – 25.0	$0.014 \pm 0.004\,(\text{stat.})\,^{+0.004}_{-0.003}\,(\text{syst.})$
25.0 – 30.0	$0.005 \pm 0.004\,(\text{stat.})\,^{+0.001}_{-0.001}\,(\text{syst.})$
30.0 – 40.0	$0.002 \pm 0.002\,(\text{stat.})\,^{+0.001}_{-0.000}\,(\text{syst.})$

Table 14: *Differential cross-section $\frac{d\sigma}{dM_X}$ for photons accompanied by at least one jet in diffractive photoproduction. (Figure 9(g–i))*

$\Delta\phi$ range (deg.)	$\frac{d\sigma}{d\Delta\phi}$ (pb deg.$^{-1}$)
$0 < z_{I\!P}^{\rm meas} \leq 1.0$	
130 – 140	$0.001 \pm 0.001\,(\text{stat.})\,^{+0.000}_{-0.000}\,(\text{syst.})$
140 – 150	$0.002 \pm 0.002\,(\text{stat.})\,^{+0.001}_{-0.001}\,(\text{syst.})$
150 – 160	$0.007 \pm 0.002\,(\text{stat.})\,^{+0.002}_{-0.001}\,(\text{syst.})$
160 – 170	$0.017 \pm 0.003\,(\text{stat.})\,^{+0.002}_{-0.003}\,(\text{syst.})$
170 – 180	$0.077 \pm 0.009\,(\text{stat.})\,^{+0.004}_{-0.009}\,(\text{syst.})$
$z_{I\!P}^{\rm meas} < 0.9$	
130 – 140	$0.001 \pm 0.001\,(\text{stat.})\,^{+0.000}_{-0.000}\,(\text{syst.})$
140 – 150	$0.002 \pm 0.002\,(\text{stat.})\,^{+0.001}_{-0.001}\,(\text{syst.})$
150 – 160	$0.006 \pm 0.002\,(\text{stat.})\,^{+0.002}_{-0.001}\,(\text{syst.})$
160 – 170	$0.015 \pm 0.003\,(\text{stat.})\,^{+0.001}_{-0.002}\,(\text{syst.})$
170 – 180	$0.038 \pm 0.005\,(\text{stat.})\,^{+0.002}_{-0.004}\,(\text{syst.})$
$z_{I\!P}^{\rm meas} \geq 0.9$	
160 – 170	$0.003 \pm 0.001\,(\text{stat.})\,^{+0.002}_{-0.001}\,(\text{syst.})$
170 – 180	$0.037 \pm 0.006\,(\text{stat.})\,^{+0.007}_{-0.006}\,(\text{syst.})$

Table 15: *Differential cross-section $\frac{d\sigma}{d\Delta\phi}$ for photons accompanied by at least one jet in diffractive photoproduction, where $\Delta\phi = |\phi^{\gamma} - \phi^{\rm jet}|$. Omitted values for $z_{I\!P}^{\rm meas} \geq 0.9$ are consistent with zero. (Figure 10(a–c))*

$\Delta\eta$ range	$\frac{d\sigma}{d\Delta\eta}$ (pb)
$0 < z_{I\!P}^{\rm meas} \leq 1.0$	
–2.9 – –2.2	$0.006 \pm 0.005\,(\text{stat.})\,^{+0.002}_{-0.001}\,(\text{syst.})$
–2.2 – –1.5	$0.018 \pm 0.028\,(\text{stat.})\,^{+0.007}_{-0.007}\,(\text{syst.})$
–1.5 – –0.8	$0.187 \pm 0.053\,(\text{stat.})\,^{+0.007}_{-0.042}\,(\text{syst.})$
–0.8 – –0.1	$0.438 \pm 0.074\,(\text{stat.})\,^{+0.029}_{-0.057}\,(\text{syst.})$
–0.1 – 0.6	$0.541 \pm 0.088\,(\text{stat.})\,^{+0.047}_{-0.067}\,(\text{syst.})$
0.6 – 1.3	$0.329 \pm 0.062\,(\text{stat.})\,^{+0.012}_{-0.044}\,(\text{syst.})$
1.3 – 2.0	$0.115 \pm 0.032\,(\text{stat.})\,^{+0.024}_{-0.013}\,(\text{syst.})$
2.0 – 2.7	$0.015 \pm 0.014\,(\text{stat.})\,^{+0.001}_{-0.002}\,(\text{syst.})$
$z_{I\!P}^{\rm meas} < 0.9$	
–2.9 – –1.5	$0.000 \pm 0.004\,(\text{stat.})\,^{+0.000}_{-0.000}\,(\text{syst.})$
–1.5 – –0.8	$0.085 \pm 0.035\,(\text{stat.})\,^{+0.002}_{-0.020}\,(\text{syst.})$
–0.8 – –0.1	$0.242 \pm 0.047\,(\text{stat.})\,^{+0.018}_{-0.029}\,(\text{syst.})$
–0.1 – 0.6	$0.343 \pm 0.058\,(\text{stat.})\,^{+0.021}_{-0.039}\,(\text{syst.})$
0.6 – 1.3	$0.220 \pm 0.048\,(\text{stat.})\,^{+0.017}_{-0.027}\,(\text{syst.})$
1.3 – 2.7	$0.040 \pm 0.012\,(\text{stat.})\,^{+0.008}_{-0.005}\,(\text{syst.})$
$z_{I\!P}^{\rm meas} \geq 0.9$	
–2.9 – –1.5	$0.028 \pm 0.013\,(\text{stat.})\,^{+0.010}_{-0.003}\,(\text{syst.})$
–1.5 – –0.8	$0.106 \pm 0.029\,(\text{stat.})\,^{+0.025}_{-0.028}\,(\text{syst.})$
–0.8 – –0.1	$0.188 \pm 0.057\,(\text{stat.})\,^{+0.035}_{-0.042}\,(\text{syst.})$
–0.1 – 0.6	$0.144 \pm 0.045\,(\text{stat.})\,^{+0.029}_{-0.030}\,(\text{syst.})$
0.6 – 1.3	$0.097 \pm 0.037\,(\text{stat.})\,^{+0.026}_{-0.027}\,(\text{syst.})$
1.3 – 2.7	$0.015 \pm 0.015\,(\text{stat.})\,^{+0.007}_{-0.011}\,(\text{syst.})$

Table 16: *Differential cross-section $\frac{d\sigma}{d\Delta\eta}$ for photons accompanied by at least one jet in diffractive photoproduction, where $\Delta\eta = \eta^{\gamma} - \eta^{\rm jet}$. (Figure 10(d–f))*

$\eta_{\max}$ range	$\frac{d\sigma}{d\eta_{\max}}$ (pb)
$0 < z_{I\!P}^{\rm meas} \leq 1.0$	
-1.0 – 0.0	$0.091 \pm 0.023\,(\text{stat.})\,^{+0.014}_{-0.101}\,(\text{syst.})$
0.0 – 0.5	$0.279 \pm 0.064\,(\text{stat.})\,^{+0.010}_{-0.042}\,(\text{syst.})$
0.5 – 1.0	$0.282 \pm 0.084\,(\text{stat.})\,^{+0.039}_{-0.034}\,(\text{syst.})$
1.0 – 1.5	$0.537 \pm 0.091\,(\text{stat.})\,^{+0.034}_{-0.069}\,(\text{syst.})$
1.5 – 2.0	$0.433 \pm 0.089\,(\text{stat.})\,^{+0.020}_{-0.062}\,(\text{syst.})$
2.0 – 2.5	$0.543 \pm 0.105\,(\text{stat.})\,^{+0.051}_{-0.069}\,(\text{syst.})$
$z_{I\!P}^{\rm meas} < 0.9$	
-1.0 – 0.0	$0.014 \pm 0.005\,(\text{stat.})\,^{+0.009}_{-0.004}\,(\text{syst.})$
0.0 – 0.5	$0.049 \pm 0.018\,(\text{stat.})\,^{+0.012}_{-0.011}\,(\text{syst.})$
0.5 – 1.0	$0.104 \pm 0.040\,(\text{stat.})\,^{+0.017}_{-0.011}\,(\text{syst.})$
1.0 – 1.5	$0.318 \pm 0.065\,(\text{stat.})\,^{+0.008}_{-0.036}\,(\text{syst.})$
1.5 – 2.0	$0.375 \pm 0.078\,(\text{stat.})\,^{+0.009}_{-0.051}\,(\text{syst.})$
2.0 – 2.5	$0.464 \pm 0.095\,(\text{stat.})\,^{+0.046}_{-0.056}\,(\text{syst.})$
$z_{I\!P}^{\rm meas} \geq 0.9$	
-1.0 – 0.0	$0.054 \pm 0.023\,(\text{stat.})\,^{+0.024}_{-0.014}\,(\text{syst.})$
0.0 – 0.5	$0.201 \pm 0.059\,(\text{stat.})\,^{+0.040}_{-0.042}\,(\text{syst.})$
0.5 – 1.0	$0.136 \pm 0.064\,(\text{stat.})\,^{+0.040}_{-0.039}\,(\text{syst.})$
1.0 – 1.5	$0.159 \pm 0.053\,(\text{stat.})\,^{+0.035}_{-0.034}\,(\text{syst.})$
1.5 – 2.0	$0.048 \pm 0.040\,(\text{stat.})\,^{+0.016}_{-0.008}\,(\text{syst.})$
2.0 – 2.5	$0.160 \pm 0.129\,(\text{stat.})\,^{+0.044}_{-0.049}\,(\text{syst.})$

Table 17: *Differential cross-section $\frac{d\sigma}{d\eta_{\max}}$ for photons accompanied by at least one jet in diffractive photoproduction. (Figure 10(g–i))*

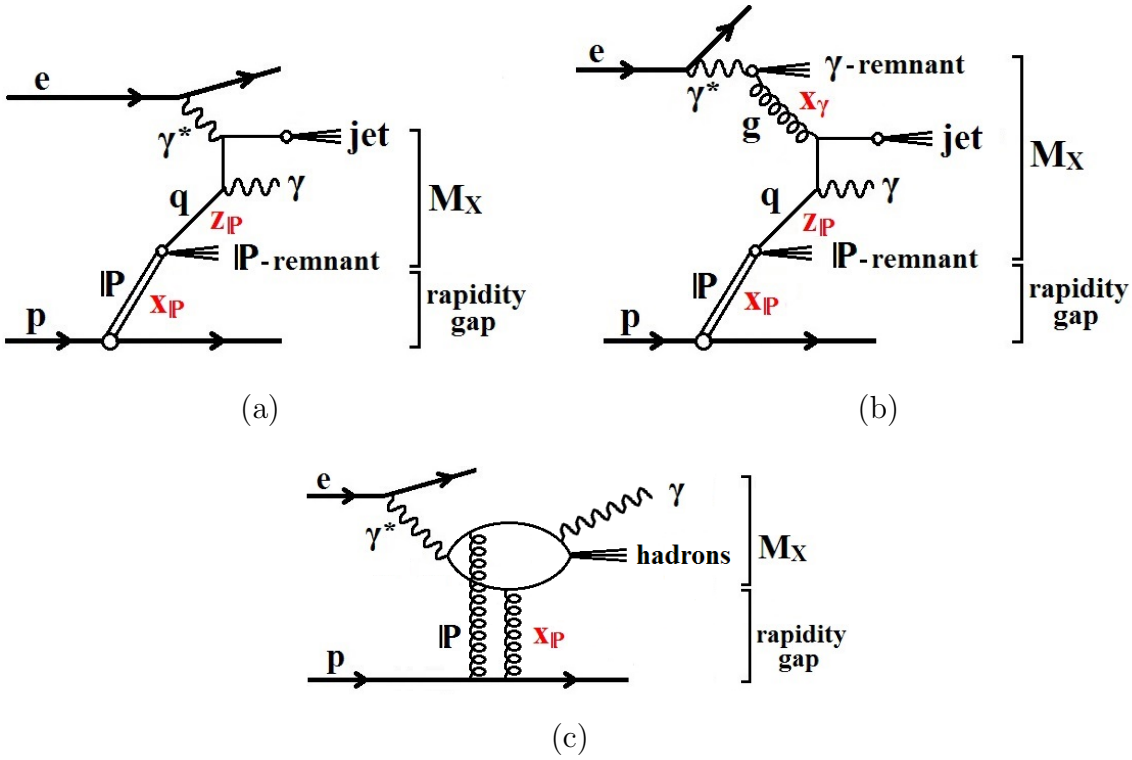

Figure 1: *Examples of diagrams for the diffractive production of a prompt photon and a jet in ep scattering from (a) direct (b) resolved photons, interacting with a resolved Pomeron. The variables are described in Section 4. (c) Example of an interaction between a direct photon and a direct Pomeron [1, 6].*

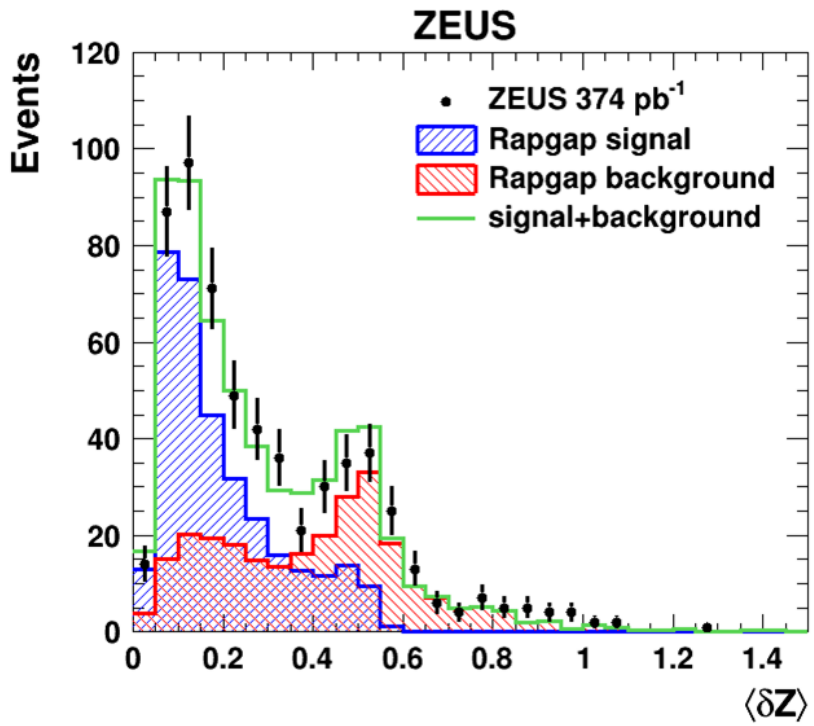

Figure 2: *Distribution of $\langle \delta Z \rangle$ for selected diffractive events with a photon candidate and at least one jet, for the full sample of HERA-II data. The error bars denote the statistical uncertainties on the data, which are compared to the fitted signal and background components from the MC. The unit of measurement of $\langle \delta Z \rangle$ is the width of one BEMC cell.*

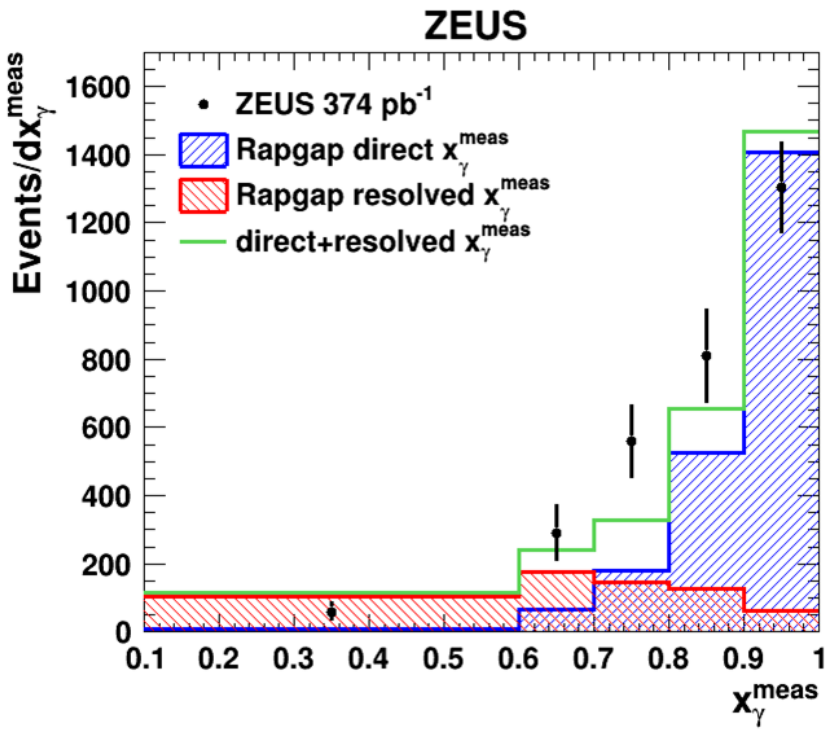

Figure 3: *HERA-II events with a photon and at least one jet as a function of* x_γ^{meas}*, per unit interval in* x_γ^{meas}*, compared to a normalised 70:30 mixture of direct:resolved photon* Rapgap *events without reweighting.*

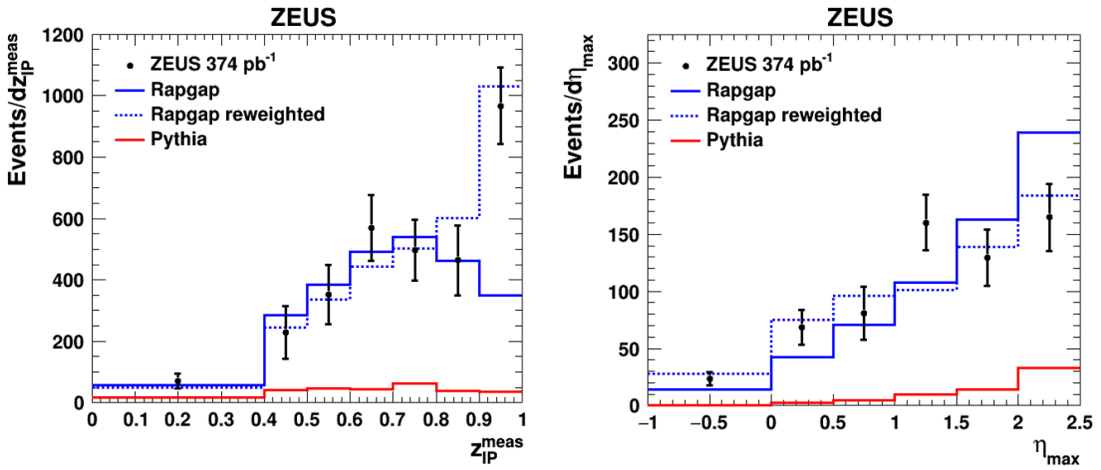

(a) (b)

Figure 4: *HERA-II events with a photon and at least one jet (a) as a function of* $z_{I\!P}^{\rm meas}$*, and (b) as a function of* $\eta_{\rm max}$*, per unit interval of each variable, compared to a 70:30* RAPGAP *mixture of direct:resolved photon events, with and without reweighting of the direct hadron-level component. The* RAPGAP *histograms are normalised to the full data sample except for the unreweighted histogram in (a), which is normalised to the data for* $z_{I\!P}^{\rm meas} < 0.9$*. The effect of a non-diffractive contribution of 10%, simulated with* PYTHIA*, is indicated by the lower solid line.*

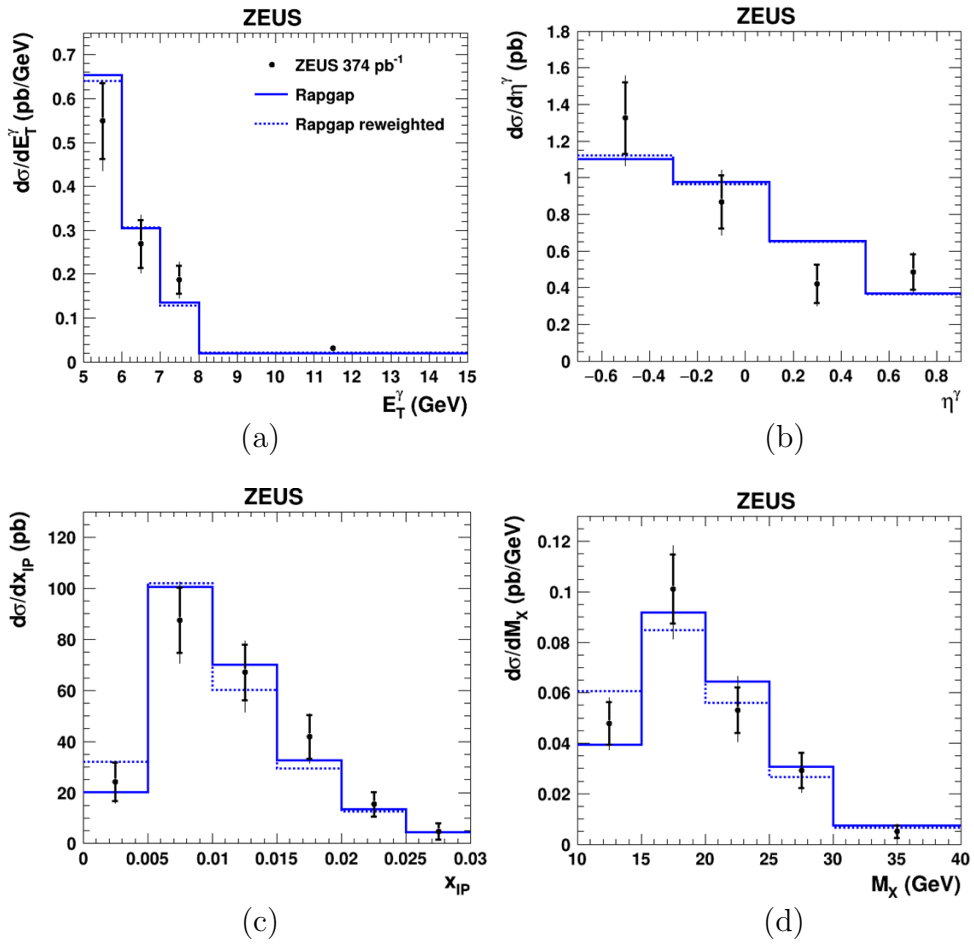

Figure 5: *Differential cross sections for inclusive isolated photon production as functions of (a) E_T^γ, (b) η^γ, (c) $x_{I\!P}$ and (d) M_X, measured with HERA-II. The kinematic region is described in the text. The inner error bars denote statistical uncertainties; the outer denote statistical with systematic uncertainties combined in quadrature. The* Rapgap *predictions are normalised to the data. (Tables 1–4)*

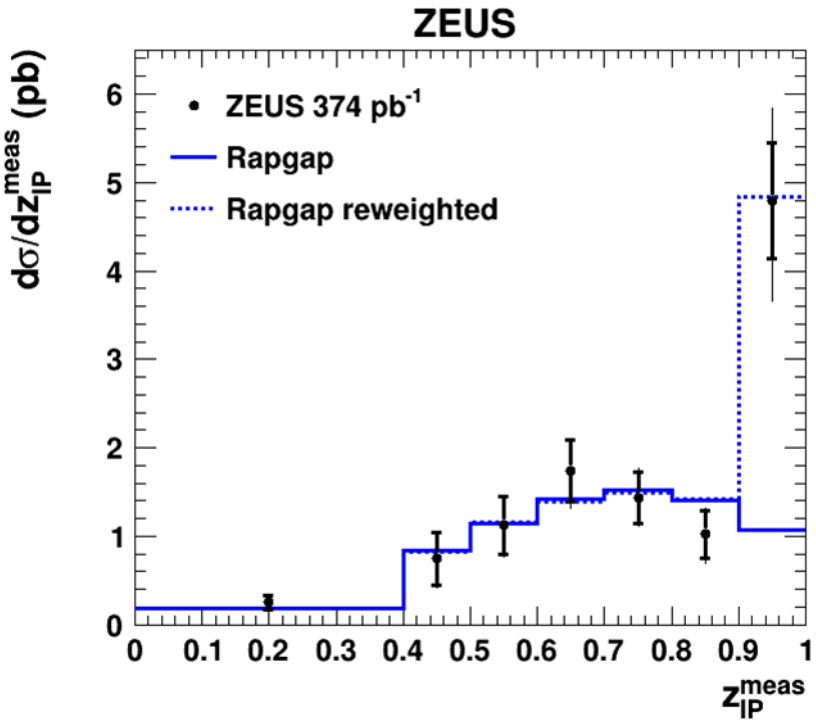

Figure 6: *Differential cross section for isolated photon production accompanied by at least one jet, as a function of* $z_{I\!P}^{\rm meas}$*, measured with HERA-II. The unreweighted* RAPGAP *prediction is normalised to the data integrated over the region* $z_{I\!P}^{\rm meas} < 0.9$*; the reweighted prediction is normalised to the full integrated data. The kinematic region is described in the text. The inner error bars denote statistical uncertainties; the outer denote statistical with systematic uncertainties combined in quadrature. (Table 5)*

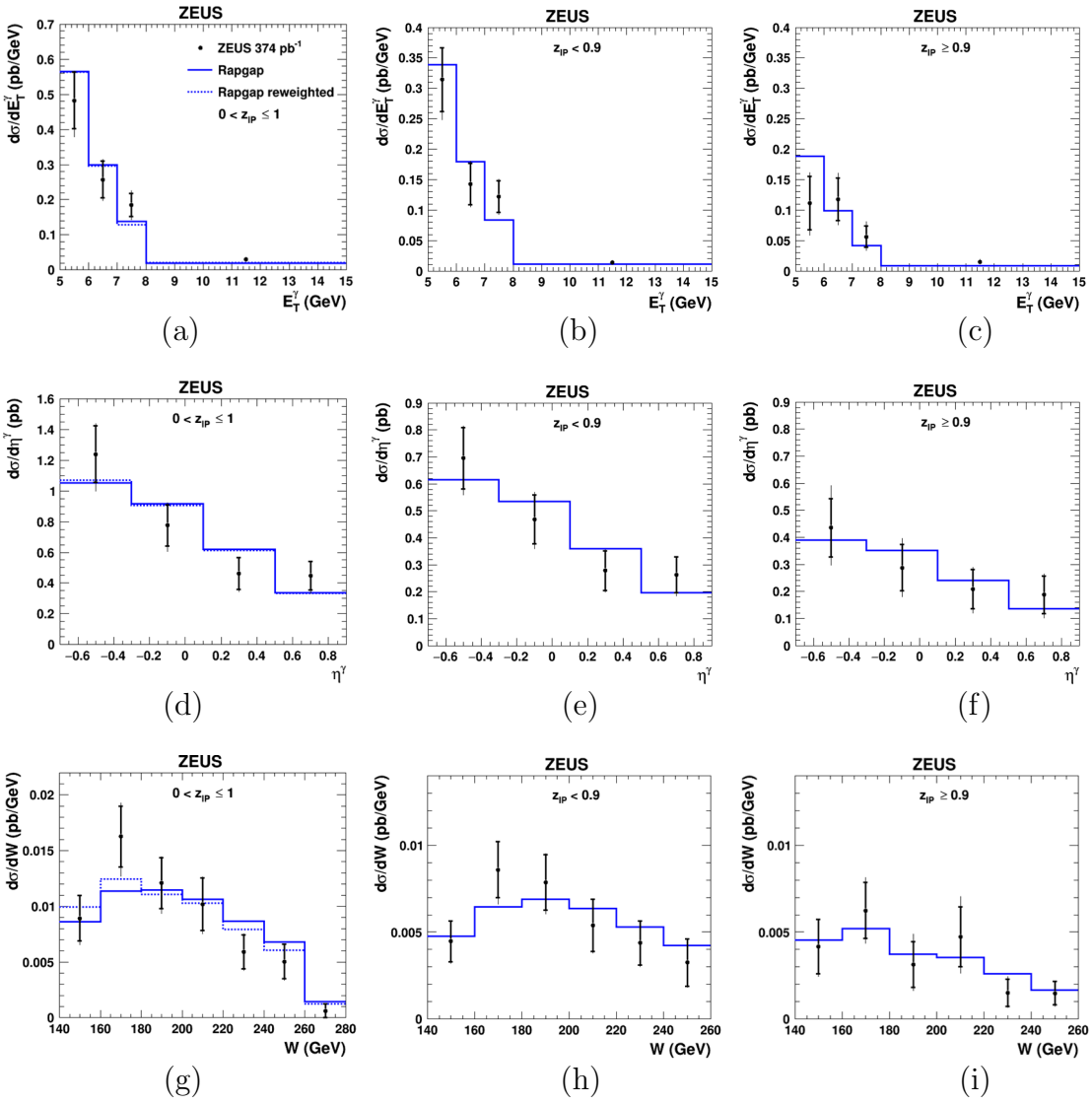

Figure 7: *Differential cross sections for isolated photon production accompanied by at least one jet, as functions of (a–c) E_T^γ, (d–f) η^γ, and (g–i) W, measured with HERA-II. Results are presented for (a, d, g) using the full $z_{I\!P}^{\rm meas}$ range, (b, e, h) $z_{I\!P}^{\rm meas} < 0.9$, and (c, f, i) $z_{I\!P}^{\rm meas} \geq 0.9$. The* RAPGAP *predictions are normalised to the data in the selected range; the reweighted prediction is shown in (a, d, g) only since in the other plots the normalisation makes the two predictions identical. The kinematic region is described in the text. The inner error bars denote statistical uncertainties; the outer denote statistical with systematic uncertainties combined in quadrature. (Tables 6–8)*

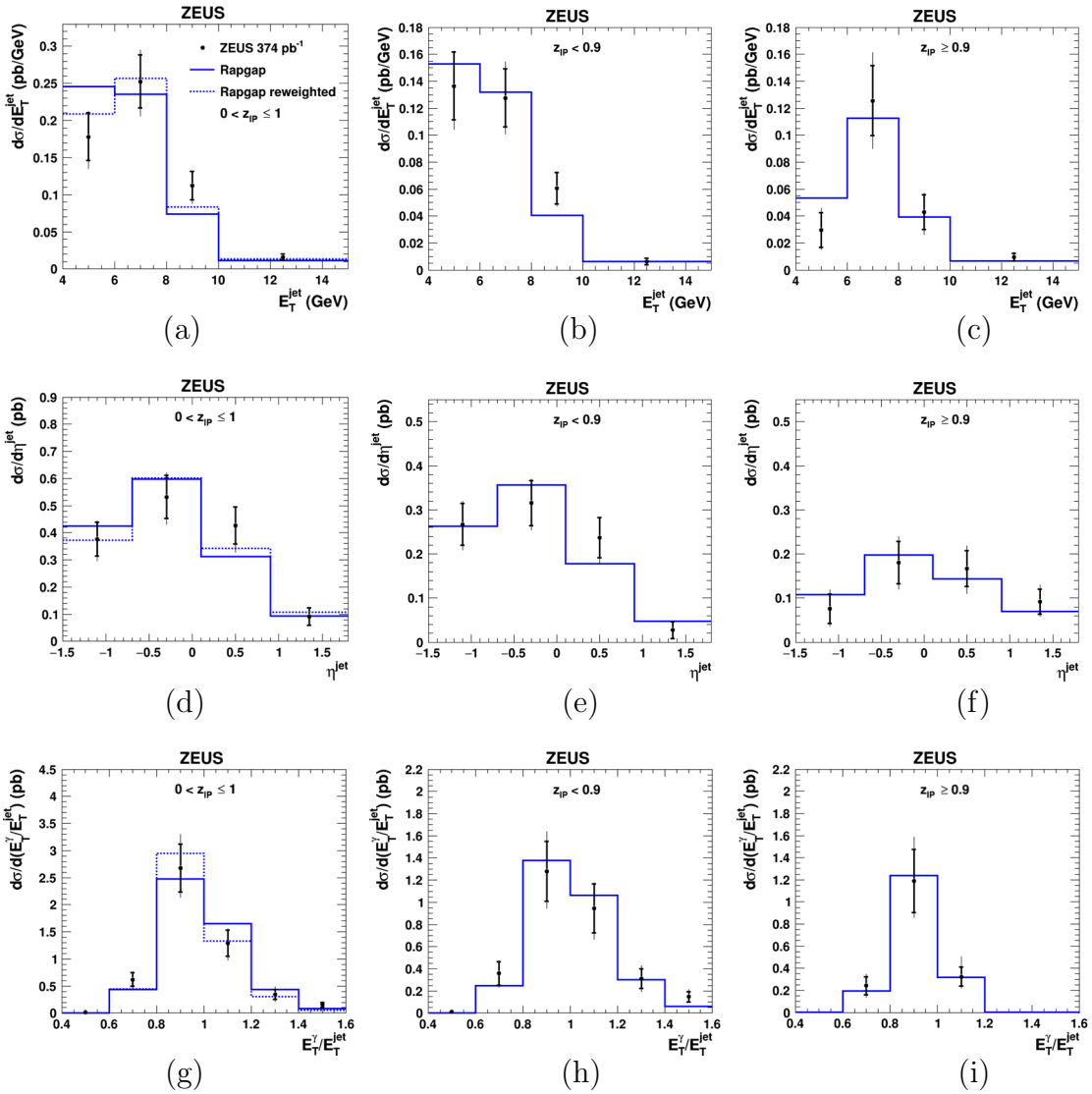

Figure 8: *Differential cross sections for isolated photon production accompanied by at least one jet, as functions of (a–c) $E_T^{\rm jet}$, (d–f) $\eta^{\rm jet}$, and (g–i) the transverse energy ratio $E_T^{\gamma}/E_T^{\rm jet}$ measured with HERA-II. Results are presented for (a, d, g) the full $z_{I\!P}^{\rm meas}$ range, (b, e, h) $z_{I\!P}^{\rm meas} < 0.9$, and (c, f, i) $z_{I\!P}^{\rm meas} \geq 0.9$. Other details as in Fig. 7. (Tables 9–11)*

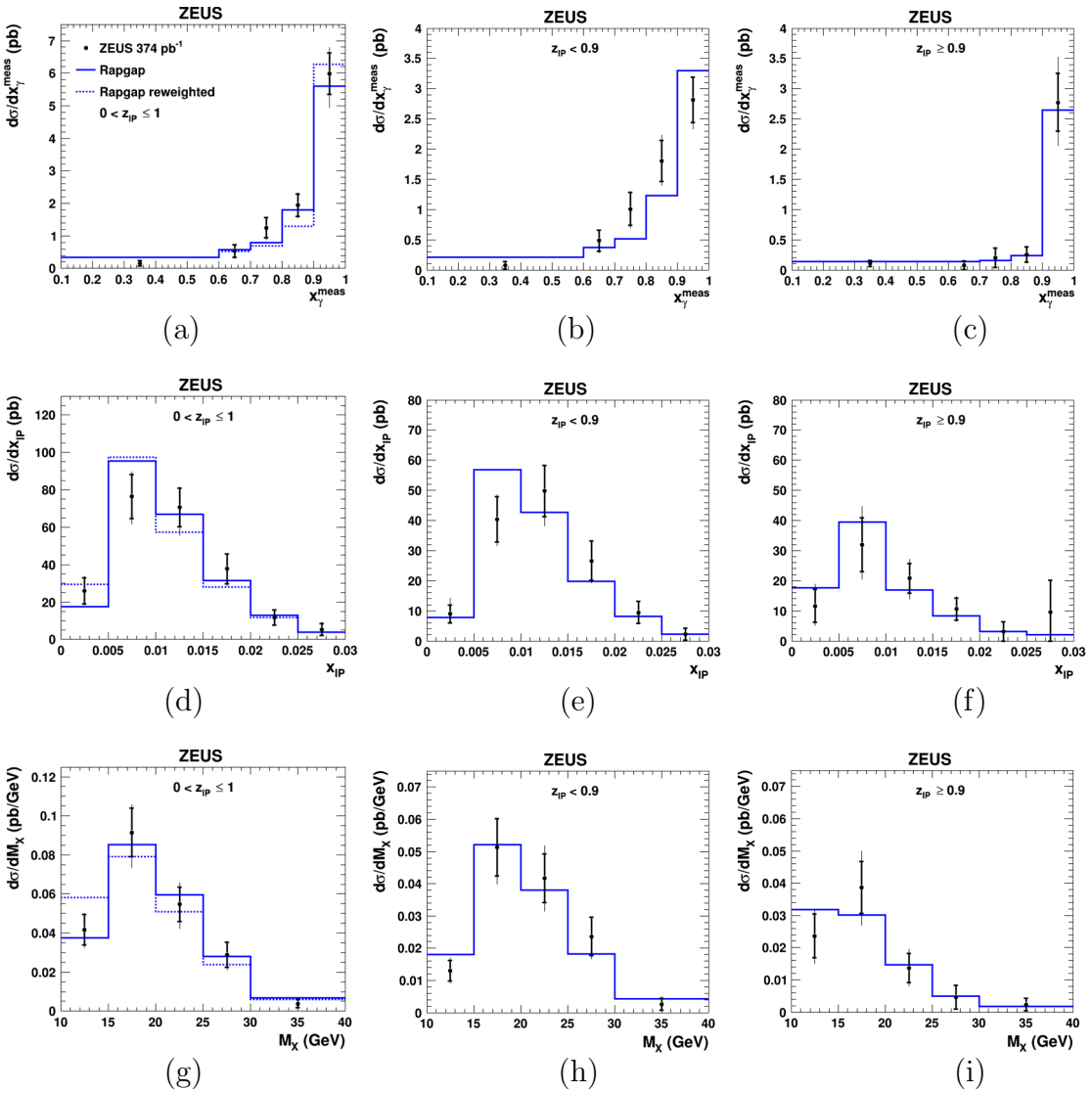

Figure 9: *Differential cross sections for isolated photon production accompanied by at least one jet, as functions of (a–c) $x_\gamma^{\rm meas}$ (d–f) $x_{I\!P}$, and (g–i) M_X, measured with HERA-II. Results are presented for (a, d, g) the full $z_{I\!P}^{\rm meas}$ range, (b, e, h) $z_{I\!P}^{\rm meas} < 0.9$, and (c, f, i) $z_{I\!P}^{\rm meas} \geq 0.9$. Other details as in Fig. 7. (Tables 12–14)*

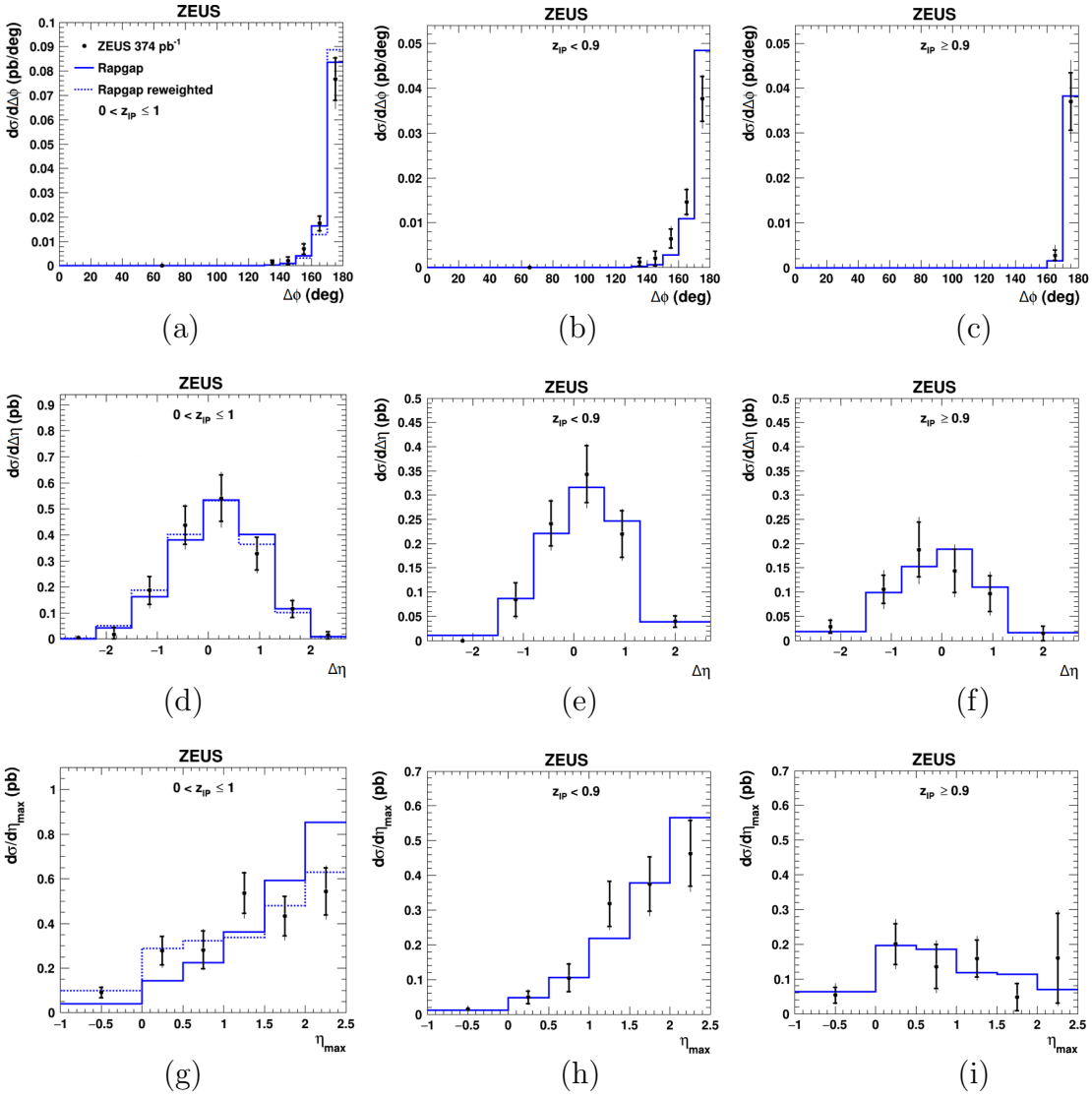

Figure 10: *Differential cross sections for isolated photon production accompanied by at least one jet, as functions of (a–c)* $\Delta\phi = |\phi^{\gamma} - \phi^{\mathrm{jet}}|$*, (d–f)* $\Delta\eta = \eta^{\gamma} - \eta^{\mathrm{jet}}$*, and (g–i)* η_{max}*, measured with HERA-II. Results are presented for (a, d, g) the full* $z_{I\!P}^{\mathrm{meas}}$ *range, (b, e, h)* $z_{I\!P}^{\mathrm{meas}} < 0.9$*, and (c, f, i)* $z_{I\!P}^{\mathrm{meas}} \geq 0.9$*. Other details as in Fig. 7. (Tables 15–17)*